Group 1 ILCs regulate T cell–mediated liver immunopathology by controlling local IL-2 availability

Valeria Fumagalli, Valentina Venzin, Pietro Di Lucia, Federica Moalli, Xenia Ficht, Gioia Ambrosi, Leonardo Giustini, Francesco Andreata, Marta Grillo, Diletta Magini, et al.

Group 1 ILCs regulate T cell–mediated liver immunopathology by controlling local IL-2 availability

Valeria Fumagalli[1,2], Valentina Venzin[1,2], Pietro Di Lucia[1], Federica Moalli[1,3], Xenia Ficht[1], Gioia Ambrosi[1], Leonardo Giustini[1], Francesco Andreata[1], Marta Grillo[1], Diletta Magini[1], Micol Ravà[1], Christin Friedrich[4], Jason D. Fontenot[5], Philippe Bousso[6], Sarah A. Gilmore[7], Shahzada Khan[7], Manuel Baca[7], Eric Vivier[8,9,10], Georg Gasteiger[4], Mirela Kuka[1,2], Luca G. Guidotti[1,2]*, Matteo Iannacone[1,2,3]*

1 3Scientific Institute, 20132 Milan, Italy. Division of Immunology, Transplantation and Infectious Diseases,
2 Vita-Salute San Raffaele University, 20132IRCCS San Raffaele Milan, Italy.
3 Experimental Imaging Centre, IRCCS San Raffaele Scientific Institute, 20132 Milan, Italy.
4 Würzburg Institute of Systems Immunology, Max Planck Research Group at the Julius-Maximiliams-Universität Würzburg, Würzburg, Germany.
5 Sangamo Therapeutics, 7000 Marina Blvd, Brisbane, CA 94005, USA.
6 Dynamics of Immune Responses Unit, Institut Pasteur, INSERM U1223, 75015 Paris, France.
7 Gilead Sci-ences, Foster City, CA 94404, USA.
8 Aix Marseille University, CNRS, INSERM, CIML, Marseille 13288, France.
9 Innate Pharma Research Laboratories, Innate Pharma, Marseille 13276, France.
10 APHM, Hôpital de la Timone, Marseille-Immunopôle, Marseille 13005, France.

*Corresponding author. Email: iannacone.matteo@hsr.it (M.I.); guidotti.luca@hsr.it (L.G.G.)

Group 1 innate lymphoid cells (ILCs), which comprise both natural killer (NK) cells and ILC1s, are important innate effectors that can also positively and negatively influence adaptive immune responses. The latter function is generally ascribed to the ability of NK cells to recognize and kill activated T cells. Here, we used multiphoton intravital microscopy in mouse models of hepatitis B to study the

intrahepatic behavior of group 1 ILCs and their cross-talk with hepatitis B virus (HBV)–specific $CD8^+$ T cells. We found that hepatocellular antigen recognition by effector $CD8^+$ T cells triggered a prominent increase in the number of hepatic NK cells and ILC1s. Group 1 ILCs colocalized and engaged in prolonged interactions with effector $CD8^+$ T cells undergoing hepatocellular antigen recognition; however, they did not induce T cell apoptosis. Rather, group 1 ILCs constrained $CD8^+$ T cell proliferation by con-trolling local interleukin-2 (IL-2) availability. Accordingly, group 1 ILC depletion, or genetic removal of their IL-2 receptor α chain,

considerably increased the number of intrahepatic HBV-specific effector $CD8^+$ T cells and the attendant immunopathology. Together, these results reveal a role for group 1 ILCs in controlling T cell–mediated liver immunopathology by limiting local IL-2 concentration and have implications for the treatment of chronic HBV infection.

INTRODUCTION

Innate lymphoid cells (ILCs) are tissue-resident immune cells that lack recombined antigen-specific receptors and do not undergo clonal selection (*1*–*5*). Hence, they react to tissue perturbations independently of antigen stimulation, and polarization of their effector function arises during their development rather than at the time of challenge (*2*). As a result of their location in peripheral tissues and effector phenotype, ILCs are poised to produce cytokines within hours of activation, in contrast to the days required for adaptive lymphocytes to be primed, expand, differentiate, and migrate from secondary lymphoid organs to peripheral tissues (*2*–*5*). In analogy with $CD4^+$ T helper cells, ILCs are classified into three subsets (group 1, group 2, and group 3) by the ability to produce effector cytokines and the requirements for specific transcriptional programs for development (*2*–*5*). Group 1 ILCs comprise natural killer (NK) cells and ILC1s; these cells require T-bet for their development and function, produce interferon-γ (IFN-γ), and have considerably overlapping expression profiles of NK cell receptors and cytokine receptors (*2*–*5*). Despite these similarities, NK cells and ILC1s are developmentally, phenotypically, and functionally distinct (*2*–*5*). NK cells are cytotoxic, circulate in the bloodstream, and require the T-box factor Eomesodermin (Eomes), whereas ILC1s have little or no cytotoxic potential, are largely tissue-resident, and can develop in the absence of Eomes (2–5). Group 2 ILCs contains a single subset, ILC2s, which are dependent on GATA binding protein-3 (GATA3) and retinoic acid-related orphan receptor-alpha (RORa), and produce type 2 cytokines, mainly interleukin-5 (IL-5) and IL-13 (2–5).

Group 3 ILCs include ILC3s and lymphoid tissue inducer cells, which are dependent on the transcription factor RORgt and can produce IL-17 and/or IL-22.

Besides rapidly producing effector cytokines in response to host, microbial, or environmental stimuli, ILCs have a complex role in directly influencing the adaptive immune response (6).

The liver is particularly enriched in group 1 ILCs, and this underscores their potential importance in the pathogenesis of infections with hepatotropic viruses such as hepatitis B virus (HBV) (*7*). HBV is a small DNA virus that causes acute and chronic liver diseases (*8*–*13*). It is widely assumed that HBV infection is noncytopathic, that it does not induce innate immune responses promptly measurable in vivo, and that T cell and antibody (Ab) responses mediate resolution of acute infection (*13*). $CD4^+$ T cells promote induction and maintenance of both $CD8^+$ T cells and neutralizing Abs, effector $CD8^+$ T ($CD8^+$ T_E) cells induce viral clearance by secreting antiviral cytokines and killing infected hepatocytes, and neutralizing Abs contain viral spread from residual cells that are not eliminated by $CD8^+$ T cells (*8*–*12*). HBV persists in the majority of neonatal/perinatal infections and a small minority of adult-onset infections, reflecting the failure of one or more of the abovementioned as-pects of the immune response (*8*–*13*). Group 1 ILCs could influence HBV pathogenesis in a number of ways (*7*, *14*). First, NK cells could be directly cytotoxic toward infected hepatocytes, as suggested by ex vivo studies in chronically infected patients (*15*). Second, NK

cells and ILC1s might produce antiviral cytokines (e.g., IFN-γ) that are known to noncytopathically inhibit viral replication (*16*). Third, group 1 ILCs might positively or negatively modulate $CD8^+$ T cell responses. NK cells and ILC1s can promote T cell responses via the secretion of cytokines [e.g., IFN-γ, tumor necrosis factor–α (TNF-α), and granulocyte-macrophage colony-stimulating factor (GM-CSF)] that support T cell differentiation (*17*). Conversely, recent data revealed that group 1 ILCs can inhibit T cell responses by directly killing $CD8^+$ T cells (*17*–*25*). However, the overall net in vivo effect of hepatic group 1 ILCs on HBV pathogenesis and liver immunopathology has, to our knowledge, not been addressed.

Here, we used multiphoton intravital microscopy, high-dimensional flow cytometry, and functional experiments in mouse models of HBV pathogenesis to explore the in vivo role of ILCs in $CD8^+$ T cell–induced liver immunopathology. We found that the mouse liver is enriched in group 1 ILCs but virtually devoid of ILC2s and ILC3s. Recognition of hepatocellular antigens by HBV-specific $CD8^+$ T_E cells induces a prominent increase in the hepatic number of group 1 ILCs, but not in ILC2s or ILC3s. Hepatic group 1 ILCs engaged in prolonged interactions with $CD8^+$ T_E cells but did not induce T cell apoptosis. Rather, group 1 ILCs competed with $CD8^+$ T_E cells for local IL-2 and, hence, restrained T cell proliferation and the attendant pathogenetic consequences.

RESULTS

Characterization and in vivo dynamics of hepatic group 1 ILCs

We started out by characterizing the frequency of ILC subsets (gating strategy shown in Fig. 1A) in the uninflamed liver of 8-week-old HBV replication–competent transgenic (HBV Tg) mice that were not experimentally manipulated. These mice express all viral proteins in hepatocytes, replicate, and secrete infectious virus but do not develop spontaneous liver pathology because replication occurs noncytopathically and endogenous HBV-specific T cells are profoundly tolerant (*26*). Consistent with previously published data in mouse models of different liver diseases (*27*, *28*), we observed that group 1 ILCs comprised ~10% of the total intrahepatic leukocyte (IHL) population (Fig. 1A). Out of group 1 ILCs, ~60 to 80% were $CD49b^+$ NK cells and ~20 to 40% were $CD49a^+$ ILC1s (Fig. 1, A to C). ILC2s and ILC3s, which are present, for example, in the airways and in the mucosa of the small intestine, respectively (fig. S1A) (*1*–*5*), were virtually absent in the liver of HBV Tg mice (Fig. 1A); therefore, they were not considered further in this study. Absolute numbers of group 1 ILCs and the relative ratio between NKs and ILC1s were virtually identical between HBV Tg mice and wild-type (WT) mice and among different genetic backgrounds (C57BL/6, BALB/c and C57BL/6 × BALB/c F_1 hybrids) (Fig. 1C and fig. S1, B to D).

We next set out to characterize the in vivo cellular dynamics of hepatic group 1 ILCs. To this end, we took advantage of $NKp46^{iCre}$ mice (*29*) to generate reporter mice, where the fluorescent protein ZsGreen is expressed by NKp46-expressing cells ($NKp46^{iCre}$;$R26^{ZsGreen}$). The frequency and absolute numbers of NK cells and ILC1s in the liver of $NKp46^{iCre}$;$R26^{ZsGreen}$ mice was comparable with those of WT mice (Fig. 1D). As expected, virtually all NK cells and ILC1s expressed ZsGreen, whereas all other IHL populations did not, with the exception of a small fraction of $NK1.1^+$ $CD3^+$ T cells (Fig. 1E). Multiphoton intravital imaging in the liver of $NKp46^{iCre}$;$R26^{ZsGreen}$ mice revealed the majority of group 1 ILCs actively crawling within liver sinusoids (movie S1 and Fig. 1, F and G) at an average speed of ~9.8 ± 0.3 μm/min (Fig. 1H) and a limited variability with regard to their instantaneous velocity (Fig. 1I). A detailed analysis of intravital image sequences showed that group 1 ILCs have an arrest coefficient (the percentage of time in which a cell has an instantaneous velocity < 3 μm/min) of ~22 ± 1 (Fig. 1J) and a meandering index (total displacement/path length of a cell track) of ~0.5 ± 0.01 (Fig. 1K). The motility coefficient, a cell's propensity to move away from its origin, of group 1 ILCs was found to be ~30.5 μm^2/min (Fig. 1L). Occasionally, group 1 ILCs showed signs of sudden U-turns between periods of normal motility (Fig. 1M). Overall, the motility parameters of group 1 ILCs were found to be remarkably similar to other cells patrolling liver sinusoids such as antigen-experienced $CD8^+$ T cells, NK T cells, and tissue-resident memory cells (*30*–*32*).

Collectively, our data indicate that, virtually, all ILCs in the liver of WT and HBV Tg mice are group 1 ILCs. Our dynamic analyses revealed that, similarly to $CD8^+$ T_E cells undergoing immune surveillance in the liver (*30*), group 1 ILCs actively crawl along liver sinusoids independently from the direction of blood flow.

Group 1 ILCs colocalize and interact with HBV-specific $CD8^+$ T_E cells

To investigate the potential interaction of endogenous group 1 ILCs with $CD8^+$ T_E cells that promote liver immunopathology, we adoptively transferred in vitro–differentiated HBV envelope-specific effector $CD8^+$ T cell receptor (TCR) transgenic T cells (Env28 T_E) (*30*, *33*) into HBV Tg mice (Fig. 2A). As expected (*30*), Env28 T_E induced a transient necroinflammatory liver disease, as assessed by serum alanine aminotransferase (ALT) elevation (Fig. 2B). We observed prominent group 1 ILC accumulation within the liver, starting as early as 2 hours and reaching the peak 2 days after Env28 T_E transfer (Fig. 2C). After day 3 post-transfer, the number of hepatic group 1 ILCs gradually declined, in parallel with serum ALT levels (Fig. 2, B and C). Among group 1 ILCs, NK cells and ILC1s increased in number up to 30 and 15 times, respectively, upon HBV-specific $CD8^+$ T_E transfer (Figure 2, D and E). By contrast, ILC2s and ILC3s remained virtually undetectable in the livers of mice undergoing T cell–mediated immunopathology (Fig. 2, F and G).

To assess the behavior of group 1 ILCs in relation to HBV-specific $CD8^+$ T_E cells within the inflamed liver, we crossed $NKp46^{iCre}$;$R26^{TdTomato}$ reporter mice with another lineage of HBV Tg mice, the major urinary protein (MUP)–core mice, which express the HBV core protein in 100% of the hepatocytes (*34*). The resulting $NKp46^{iCre}$;$R26^{TdTomato}$;MUP-core mice were cotransferred with in vitro–differentiated fluorescent HBV core–specific T_E (Cor93 T_E) cells and with T_E cells specific for an irrelevant antigen (P14 T_E) (Fig. 2H). Liver multiphoton intravital microscopy (movie S2) and confocal immunofluorescence histology (Fig. 2I) were carried out between 2 and 48 hours after cell injection. Static and dynamic imaging revealed that hepatic group 1 ILCs engaged in stable, prolonged interactions with antigen-recognizing Cor93 T_E, whereas they formed much fewer and shorter contacts with irrelevant P14 T_E cells, which crawled along liver sinusoids (Fig. 2I and movie S2). Quantification of cell-to-cell contacts confirmed that, 6 hours after T_E injection into $NKp46^{iCre}$; $R26^{TdTomato}$; MUP-core mice—a time point in which most Cor93 T_E already encountered cognate Ag(*30*)—hepatic group 1 ILCs colocalized with ~12 ± 1.6% of Cor93 T_E and just with ~5 ± 1.2% of P14 T_E. We observed less than 3% of hepatic group 1 ILC colocalization with either HBV-specific or irrelevant

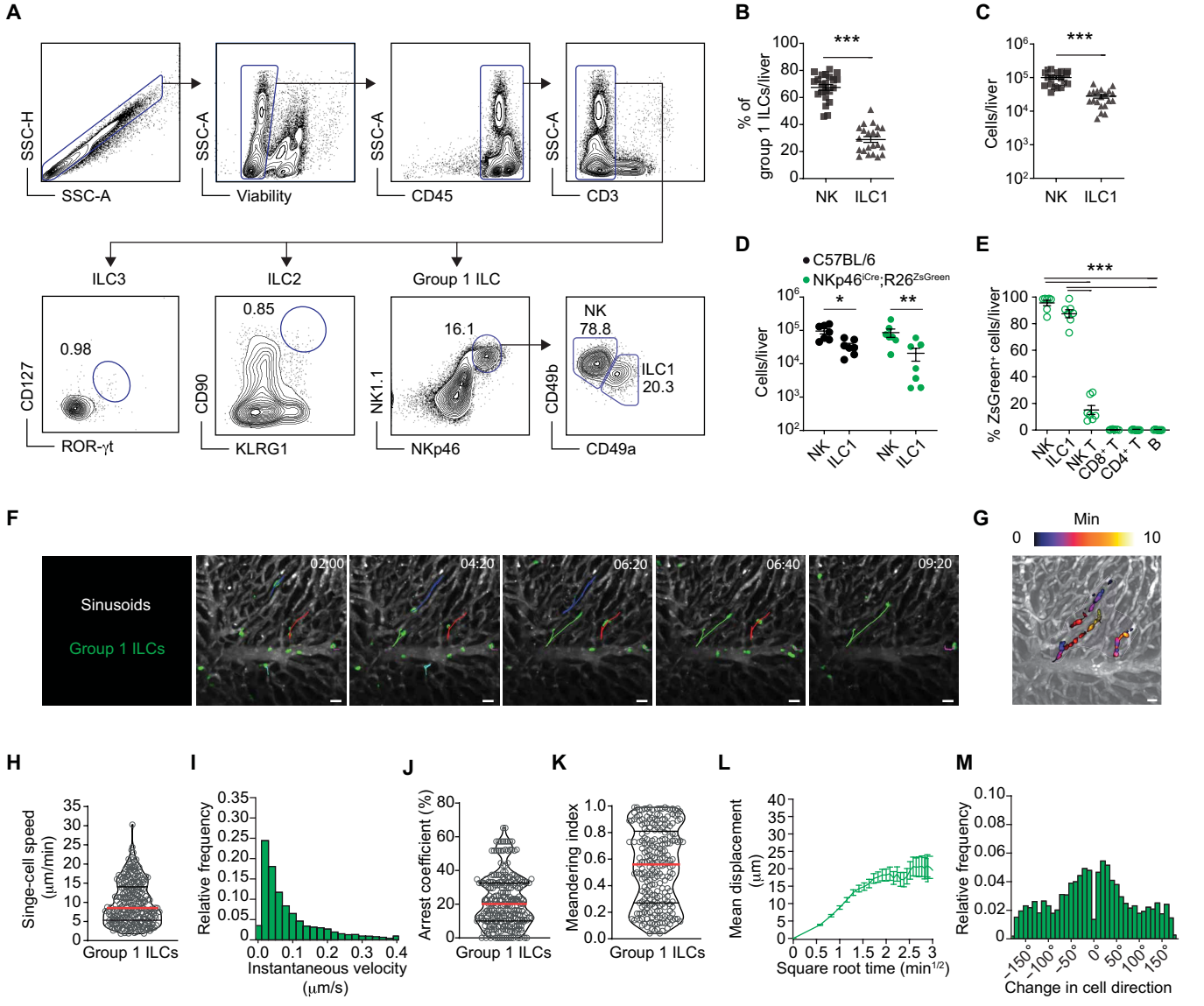

Fig. 1. Characterization and in vivo dynamics of hepatic group 1 ILCs. (**A**) The flow cytometry gating strategy used for the identification of ILC subsets is shown. Live, $CD45^+CD3^-$ cells in the liver of HBV Tg mice were further analyzed for concomitant expression of NK1.1 and NKp46 (group 1 ILCs), CD90 and KLRG1 (ILC2s), and CD127 and ROR-γt (ILC3s). Group 1 ILCs were further clustered in $CD49b^+CD49a^-$ NK cells and $CD49b^-CD49a^+$ ILC1s. Side scatter pulse height, SSC-H; side scatter area, SSC-A. (**B** and **C**) Frequencies (B) and absolute numbers (C) of hepatic NK cells and ILC1s in HBV Tg mice ($n = 22$). (**D**) Absolute numbers of hepatic NK cells and ILC1s in C57BL/6 mice (black dots, $n = 7$) and $NKp46^{iCre};R26^{ZsGreen}$ mice (green dots, $n = 7$). (**E**) Percentage of the indicated cell types expressing ZsGreen in the liver of $NKp46^{iCre};R26^{ZsGreen}$ mice ($n = 7$). (**F**) Multiphoton intravital microscopy time lapse in the liver of a $NKp46^{iCre};R26^{ZsGreen}$ mouse injected with Qtracker quantum dots to visualize the blood vessels (white). Group 1 ILCs are depicted in green, and cell tracks are indicated. Elapsed time in minutes:seconds. Scale bars, 20 μm. (**G**) Superposition of intravital microscopy frames with color coding (from blue to yellow) for the occupancy time of each pixel showing selected $ZsGreen^+$ cells moving into sinusoids of $NKp46^{iCre};R26^{ZsGreen}$ mice. (**H** to **M**) Quantitative analyses of group 1 ILC behavior in the mouse liver. Average cell velocity per track (H); instantaneous 3D velocity (I); arrest coefficient, calculated for a threshold of 3 μm/min (J); meandering index (K) (0 = completely condensed or circular cell tracks; 1 = perfectly straight cell tracks); mean displacement of group 1 ILCs plotted as a function of the square root of time (L) (slope = 30.5 μm^2/min and represents the motility coefficient); and quantification of turning angle changes (M). Data in (B) to (E) are expressed as means ± SEM and are representative of at least three independent experiments. Data in (F) to (M) are from five mice in five experiments, circles represent a cell track, red bars indicate median values, and black bars indicate quartiles. A total of 238 group 1 ILC tracks were analyzed. $^*P < 0.05$, $^{**}P < 0.01$, and $^{***}P < 0.001$; Mann-Whitney *U* test (B to D) and one-way ANOVA followed by Sidak's multiple comparisons test, comparison between the mean of each group with the mean of NK cells or ILC1s (E).

T_E in noninflamed WT mice (Fig. 2J). In line with these findings, multiphoton intravital imaging of the liver showed a reduction in group 1 ILC motility and straightness over time (Fig. 2, K and L). Further analyses revealed that up to 20% of interactions between group 1 ILCs and Cor93 T_E lasted longer than 20 min, whereas fewer than 8% of interactions with P14 T_E were maintained for this time (Fig. 2M). In summary, these observations indicate that hepatic group 1 ILCs exhibit an intrasinusoidal crawling behavior and engage in stable, prolonged interactions with $CD8^+$ T_E cells recognizing hepatocellular antigens.

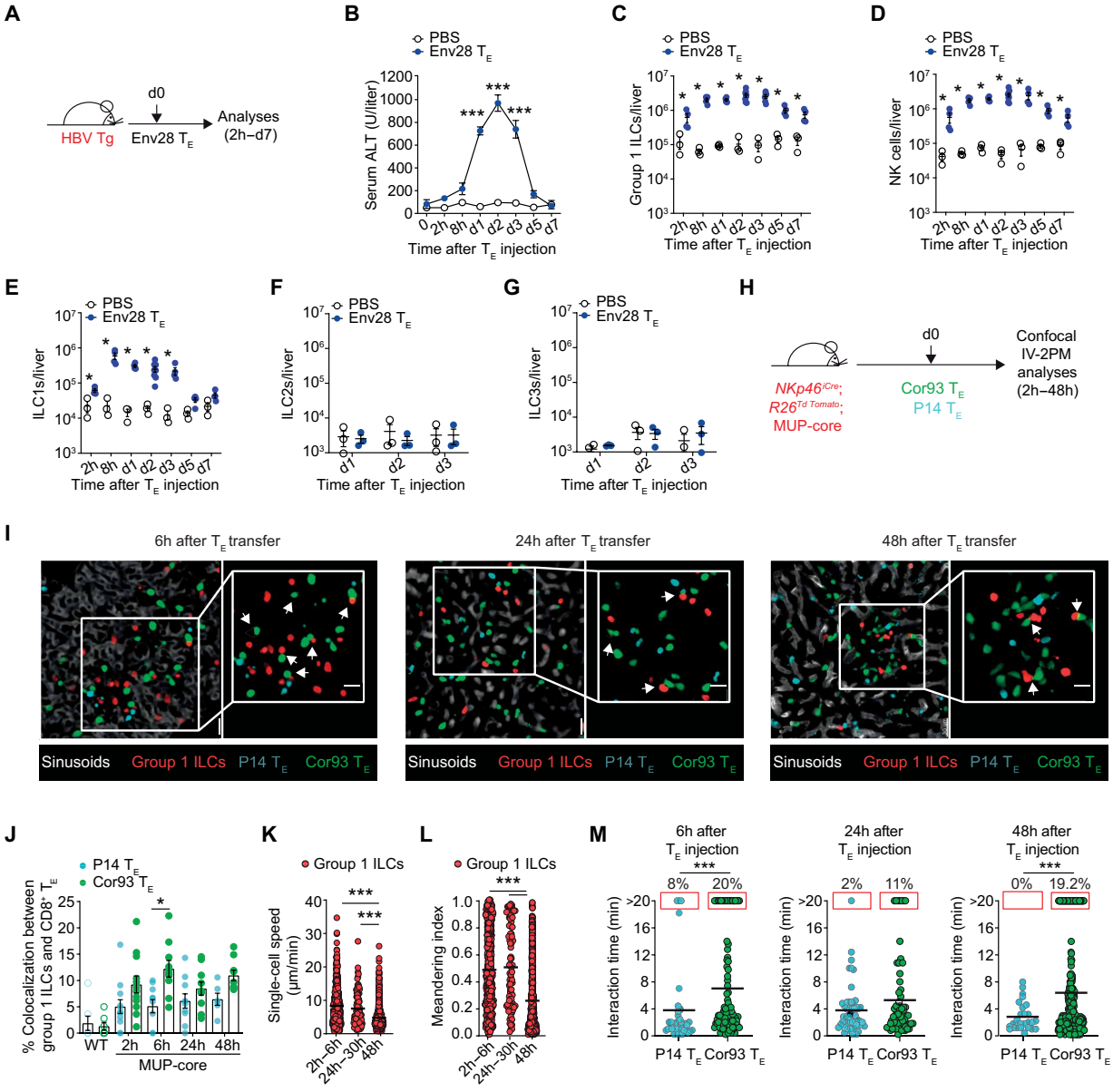

Fig. 2. Group 1 ILCs colocalize and interact with HBV-specific CD8$^+$ T_E cells. (**A**) Schematic representation of the experimental setup. HBV Tg mice received 10^7 HBsAg-specific T_E cells (Env28 T_E). Livers were collected and analyzed from 2 hours to 7 days after Env28 T_E transfer. (**B**) Serum transaminase activity (ALT; U/liter) measured in HBV Tg mice after Env28 T_E injection (blue dots, $n = 4$ to 8) or in PBS-treated control mice (white dots, $n = 3$). (**C** to **E**) Absolute numbers of total group 1 ILCs (C), NK cells (D), and ILC1s (E) in the liver of HBV Tg mice at the indicated time points after Env28 T_E transfer. Data are expressed as means ± SEM and are representative of at least four independent experiments. (**F** and **G**) Absolute numbers of ILC2s (F) and of ILC3s (G) in the liver of HBV Tg mice at the indicated time points after Env28 T_E transfer. Data are expressed as means ± SEM and are representative of at least two independent experiments. (**H**) Schematic representation of the experimental setup. NKp46$^{iCre+/-}$;R26$^{TdTomato+/-}$;MUP-core mice received 10^7 fluorescent Cor93 T_E (green) and 10^7 fluorescent control P14 T_E (cyan). (**I**) Representative confocal immunofluorescence micrographs of liver sections from the indicated mice 6, 24, and 48 hours after T cell transfer. Group 1 ILCs are depicted in red, Cor93 T_E in green, and control P14 T_E in cyan. Sinusoids were identified as Lyve-1$^+$ cells and are depicted in white. White boxes represent the magnification. Arrows indicate colocalization between group 1 ILCs (red) and Cor93 T_E (green). Scale bars, 30 μm (image) and 15 μm (magnification). (**J**) Quantification of the colocalization between group 1 ILCs and the indicated effector T cells at different time points after T cell transfer in NKp46$^{iCre+/-}$;R26$^{TdTomato+/-}$ mice (WT; $n = 7$) or NKp46$^{iCre+/-}$;R26$^{TdTomato+/-}$;MUP-core mice (MUP-core; $n = 6$ to 12). Circles represent the mean of the number of interactions calculated in different fields of view for the same mouse. Data are representative of at least five independent experiments. (**K** to **M**) Multiphoton intravital microscopy analysis in the liver of NKp46$^{iCre+/-}$;R26$^{TdTomato+/-}$;MUP-core mice injected with fluorescent T_E (2 to 6 hours, $n = 6$; 24 to 30 hours, $n = 4$; 48 hours, $n = 3$). Single-cell speed (K) and meandering index (L) of group 1 ILCs at the indicated time points. A total of 578 (2 to 6 hours), 82 (24 to 30 hours), and 625 (48 hours) group 1 ILCs tracks were analyzed. (M) Quantification of the interaction time between group 1 ILCs and the indicated effector T cells at different time points after transfer. Red boxes indicate the percentage of cells that are interacting for more than 20 min. Data are representative of at least three independent experiments. *$P < 0.05$ and ***$P < 0.001$; two-way ANOVA followed by Sidak's multiple comparisons test, stars indicate significant differences among groups for each time point (B); Kruskal-Wallis test (K and L); two-tailed Mann-Whitney *U* test (C to G) (comparison between blue and white dots for each time point); two-tailed Mann-Whitney *U* test (J and M) (comparison between Cor93 T_E and P14 T_E).

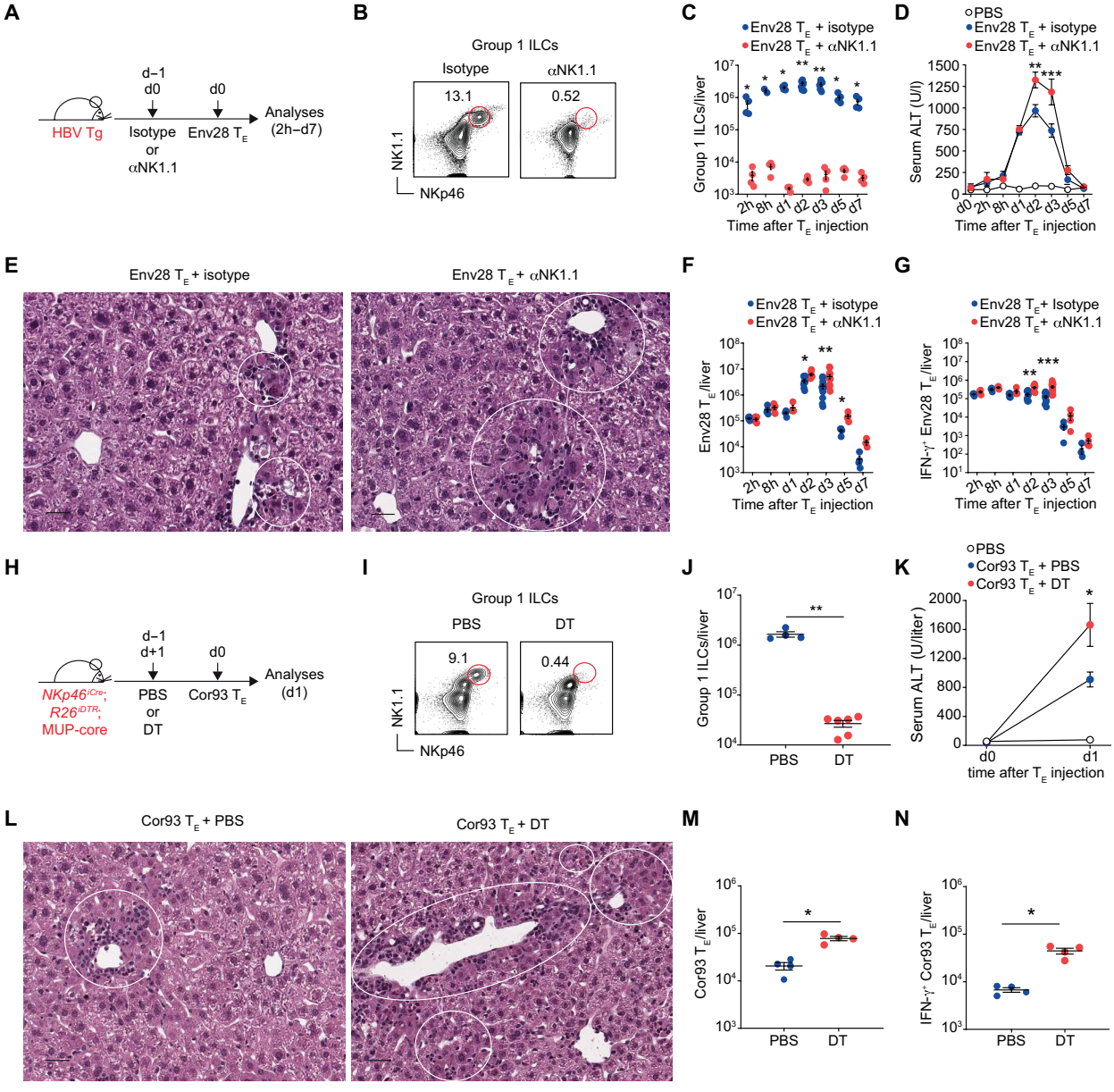

Fig. 3. Group 1 ILCs limit T cell–mediated liver immunopathology. (**A**) Schematic representation of the experimental setup. HBV Tg mice were injected with αNK1.1-depleting Abs or isotype control before receiving 10^7 HBsAg-specific $CD8^+$ T_E cells (Env28 T_E). Livers were collected and analyzed from 2 hours to 7 days after Env28 T_E transfer as indicated in the next panels. (**B**) Representative flow cytometry plot of group 1 ILCs obtained from the liver of the indicated mice 2 days after αNK1.1 treatment. (**C**) Absolute numbers of group 1 ILCs in the liver of HBV Tg mice receiving αNK1.1-depleting Abs (αNK1.1; $n = 4$, red dots) or isotype control (Isotype; $n = 4$ to 8, blue dots) at the indicated time points after Env28 T_E transfer. (**D**) Serum transaminase activity (ALT; U/liter) in the indicated HBV Tg mice after Env28 T_E injection. Comparison among mice treated with the αNK1.1-depleting Abs (αNK1.1; $n = 4$, red dots) or isotype control (Isotype; $n = 4$ to 8, blue dots). Control mice treated with PBS are also shown (PBS; $n = 2$, white dots). (**E**) Representative H&E micrographs of liver sections from mice treated with isotype control (left) or αNK1.1 Abs (right) 2 days after Env28 T_E injection. White circles indicate necroinflammatory foci. Scale bars, 20 μm. (**F** and **G**) Absolute numbers of Env28 T_E cells (F) and of IFN-γ^+ Env28 T_E cells (G) in the liver of the indicated mice at different time points after Env28 T_E transfer. Data are expressed as means ± SEM and are pooled from two independent experiments. (**H**) Schematic representation of the experimental setup. NKp46$^{iCre+/-}$; R26$^{iDTR+/-}$; MUP-core mice were injected with DT every 48 hours starting 1 day before receiving 10^7 HBcAg-specific T_E cells (Cor93 T_E). Livers were collected and analyzed 1 day after Cor93 T_E transfer. (**I**) Representative flow cytometry plot of group 1 ILCs obtained from the liver of the indicated mice 1 day after DT treatment. (**J**) Absolute numbers of group 1 ILCs in the liver of mice injected with DT ($n = 3$ to 4, red dots) or PBS ($n = 3$ to 5, blue dots) after Cor93 T_E transfer. (**K**) Serum transaminase activity (ALT; U/liter) in the indicated mice after Cor93 T_E injection. Statistical analysis was performed by comparing mice with or without DT treatment. Control, PBS-treated mice are indicated in white ($n = 4$). (**L**) Representative H&E micrographs of liver sections from mice treated with PBS (left) and DT (right) 1 day after Cor93 T_E injection. White circles indicate necroinflammatory foci. Scale bars, 20 μm. (**M** and **N**) Absolute numbers of Cor93 T_E cells (M) and of IFN-γ^+ Cor93 T_E cells (N) in the liver of the indicated mice after T_E transfer are shown. Data are expressed as means ± SEM and are representative of at least two independent experiments. *$P < 0.05$, **$P < 0.01$, and ***$P < 0.001$; two-tailed Mann-Whitney U test (C, F, G, J, M, and N) (comparison between blue and red dots for each time point) and two-way ANOVA followed by Sidak's multiple comparisons test (D and K) (comparison between blue and red dots for each time point).

Group 1 ILCs limit T cell–mediated liver immunopathology

We next turned our attention to the possible consequences of the observed interactions between hepatic group 1 ILCs and HBV-specific $CD8^+$ T_E cells. To this end, we treated HBV Tg mice with anti-NK1.1 (αNK1.1)–depleting Abs before Env28 T_E transfer (Fig. 3A). As expected, Ab treatment resulted in efficient and durable group 1 ILC depletion (Fig. 3, B and C) but also in a significant reduction in hepatic $NK1.1^+$ $CD3^+$ T cells (fig. S2, A and B). Group 1 ILC depletion resulted in a more severe liver disease, as assessed by the increase in transaminase activity (Fig. 3D) and by the presence of larger and more numerous necroinflammatory foci (Fig. 3E). Consistently with this, we found that group 1 ILC depletion led to an increase in hepatic IFN-γ–producing Env28 T_E accumulation (Fig. 3, F and G). Overall, these data indicate that hepatic group 1 ILCs limit hepatic HBV-specific $CD8^+$ T_E accumulation and the attendant immunopathology.

To exclude any possible off-target effects of the depleting Ab, we sought an alternative approach to eliminate group 1 ILCs. This was achieved by crossing $NKp46^{iCre}$;$R26^{iDTR}$ mice (*29*) with MUP-core mice (Fig. 3H). Diphtheria toxin (DT) administration to $NKp46^{iCre}$;$R26^{iDTR}$;MUP-core mice resulted in efficient depletion of group 1 ILCs (Fig. 3, I and J) but not of $NK1.1^+$ $CD3^+$ T cells (fig. S2, C and D). One day after DT [or phosphate-buffered saline (PBS)] treatment, we adoptively transferred Cor93 T_E to $NKp46^{iCre}$;$R26^{iDTR}$;MUP-core mice (Fig. 3H). In accordance with the data described in Fig. 3 (D to G), DT-mediated group 1 ILC depletion caused a more severe liver immunopathology and increased intrahepatic Cor93 T_E cell accumulation (Fig. 3, K to N).

Group 1 ILCs do not affect intrahepatic $CD8^+$ T_E cell death

We next sought to identify the mechanisms by which group 1 ILCs limit T cell–mediated liver immunopathology. We first asked whether hepatic group 1 ILCs might limit liver immunopathology by interfering with HBV-specific $CD8^+$ T_E cell recruitment and/or hepatocellular antigen recognition. To address this, we depleted group 1 ILCs from MUP-core mice 1 day after HBV-specific T_E transfer, a time point in which the vast majority of T_E liver homing and antigen recognition has already taken place (fig. S3A) (*30*). As shown previously, the number of hepatic group 1 ILCs significantly increased upon HBV-specific T_E injection and they were efficiently depleted by αNK1.1 treatment (fig. S3B). The depletion of group 1 ILCs 1 day after T cell transfer led to an increase in liver disease (fig. S3, C and D) that was associated with a higher intrahepatic accumulation of IFN-γ–producing Cor93 T_E (fig. S3, E and F). These data indicate that hepatic group 1 ILCs can restrain T cell–mediated immunopathology by acting downstream of T cell recruitment or hepatocellular antigen recognition and call for further investigation of the mechanisms whereby group 1 ILCs affect intrahepatic T cell abundancy.

Considering the finding that hepatic group 1 ILCs are in direct contact with HBV-specific $CD8^+$ T_E cells (Fig. 2, I, J, and M) and the notion that group 1 ILCs, particularly NK cells, were suggested to directly kill $CD8^+$ T cells in a number of experimental settings (*21*, *23–25*, *35*), we explored the possibility that HBV-specific $CD8^+$ T_E cells might die as a consequence of the interaction with group 1 ILCs. First, we quantified activated caspases (as a readout for apoptosis) in Cor93 T_E isolated from the livers of MUP-core mice that received αNK1.1-depleting Ab (or isotype control) before T cell transfer (Fig. 4A). Activated caspases in apoptotic Cor93 T_E were irreversibly bound by the fluorescein isothiocyanate (FITC)–labeled caspase inhibitor Val-Ala-Asp-fluoromethyl ketone (VAD-FMK) and detected by flow cytometry (Fig. 4B). With this method, we were able to detect apoptotic Cor93 T_E in the livers of MUP-core mice, and their frequency paralleled liver disease severity, reaching a peak of ~44% (Fig. 4, B and C). However, we failed to observe any differences in Cor93 T_E apoptosis between MUP-core mice that were depleted of group 1 ILCs and control animals (Fig. 4, B and C).

To assess T cell death with an alternative method, we took advantage of a Förster resonance energy transfer (FRET)–based reporter of caspase-3 activity (*36*). Briefly, in vitro–differentiated Cor93 T_E (Cor93 T_E) cells were transduced with a fluorescent probe containing the cyan (CFP) and the yellow (YFP) fluorescent protein linked by a peptide (DEVD) cleavable by activated caspase-3 (Fig. 4D). Caspase-3 activation in apoptotic cells results in CFP → YFP FRET disruption and in the detection of a CFP^+ YFP^- signal. Control Cor93 T_E cells were transduced with a different probe, in which the peptide linker (DEVG) is not cleavable by activated caspase-3 (Fig. 4D). We confirmed that effector T cell differentiation was not affected by transduction with the abovementioned probes, as assessed by the ability of Cor93 T_E to express IFN-γ upon in vitro cognate peptide simulation (fig. S4A). The sensitivity and specificity of this method in detecting T cell apoptosis was assessed by inducing activation-induced cell death upon in vitro stimulation with the cognate peptide for 6 hours. As expected (*37*), FRET loss and emission of a CFP^+ YFP^- signal were readily detected in DEVD-transduced T cell, whereas no changes were detected in control, DEVG-transduced T cell (fig. S4B). We then adoptively transferred DEVG- or DEVD-transduced Cor93 T_E to $NKp46^{iCre}$;$R26^{iDTR}$;MUP-core mice that received DT (or PBS) before T cell injection (Fig. 4E). As before, we were able to detect apoptotic Cor93 T_E with this method (Fig. 4F); however, the frequency of CFP^+ YFP^- apoptotic Cor93 T_E and the apoptotic index (ratio between the percentage of dead cells and the percentage of live cells) were similar in mice treated with DT or PBS (Fig. 4, F and G). As expected, no CFP^+ YFP^- signal was detected in control, DEVG-transduced Cor93 T_E (Fig. 4, F and G). The data, obtained with an alternative independent method, confirm that group 1 ILCs do not affect intrahepatic HBV-specific $CD8^+$ T_E cell apoptosis.

To confirm this further, we considered that the cytotoxic activity of NK cells toward $CD8^+$ T cells relies mostly on perforin (*20–22*, *24*, *25*). Irradiated MUP-core mice were thus reconstituted with perforin-deficient ($Prf^{-/-}$) or WT bone marrow (BM) followed, 8 weeks later, by the injection of αNK1.1 Ab (or isotype control) before Cor93 T_E transfer (Fig. 4H). With this approach, NK cells from recipient mice would lack the ability to release perforin, and the only perforin source would come from the adoptively transferred Cor93 T_E. Hepatic group 1 ILC expansion upon T_E injection was not significantly different in WT- and $Prf^{-/-}$-reconstituted mice (Fig. 4I). $Prf^{-/-}$- and WT-reconstituted mice did not differ in their capacity to support the expansion of IFN-γ–producing Cor93 T_E (Fig. 4, J and K). Moreover, αNK1.1 treatment had a similar effect on intrahepatic Cor93 T_E accumulation and on the attendant immunopathology in $Prf^{-/-}$- and WT-reconstituted mice (Fig. 4, J and K, and fig. S5A).

Previous reports have shown that NK cells can kill activated T cells upon engagement of natural cytotoxicity triggering receptor 1 (NCR1) (*24*, *38–40*). We thus reconstituted irradiated MUP-core mice with $Ncr1^{-/-}$ or WT BM followed, 8 weeks later, by the injection of αNK1.1 Ab (or isotype control) before Cor93 T_E transfer (Fig. 4L). The number of group 1 ILCs after T_E injection increased

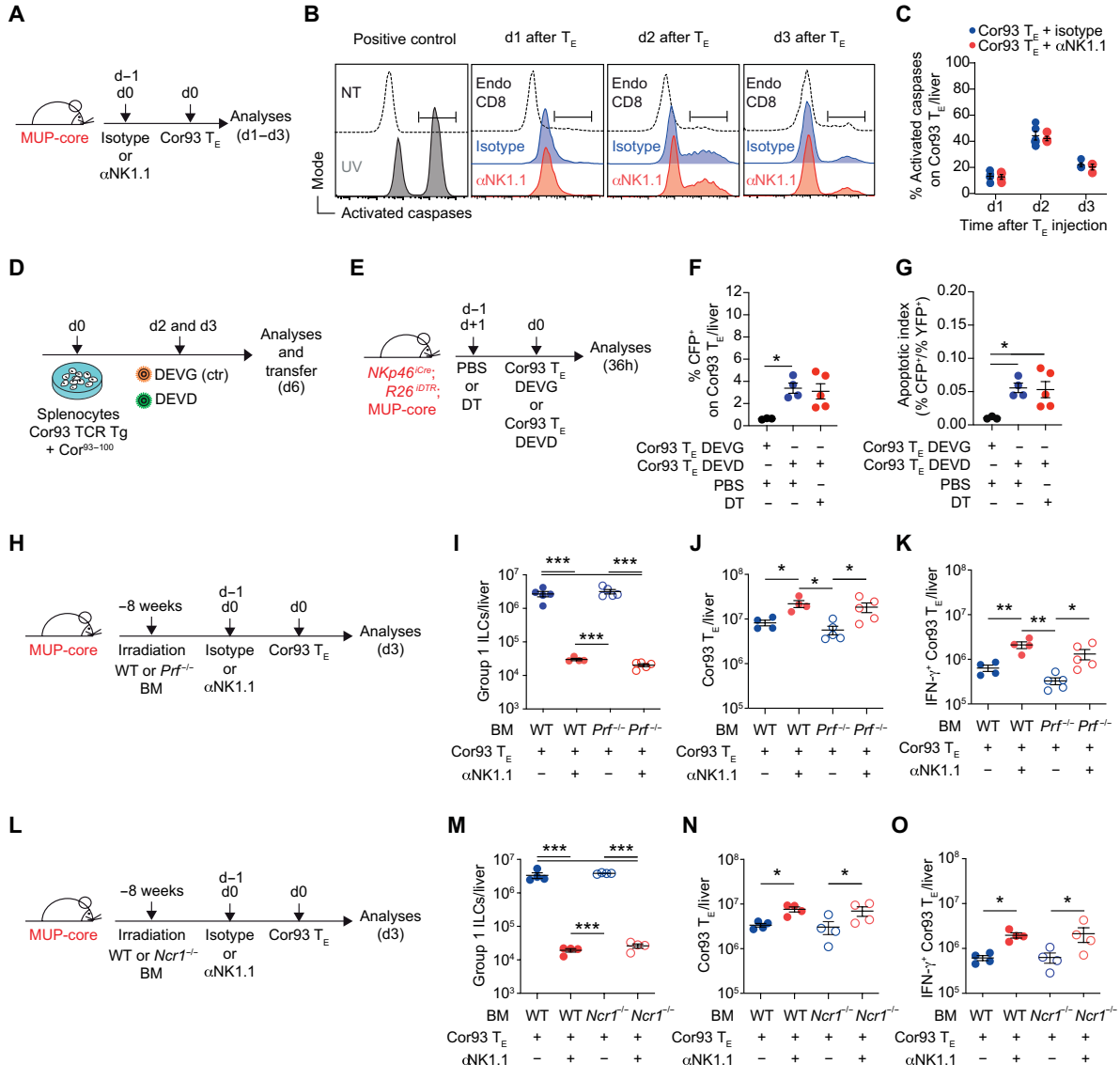

Fig. 4. Group 1 ILCs do not affect intrahepatic CD8$^+$ T$_E$ cell death. (**A**) MUP-core mice were injected with αNK1.1-depleting Abs or isotype control before receiving 10^7 HBV core–specific CD8$^+$ T$_E$ cells (Cor93 T$_E$). Livers were collected and analyzed 1 to 3 days after Cor93 T$_E$ transfer. (**B** and **C**) Representative histograms (B) and percentage (C) of Cor93 T$_E$ cells that stained positive for activated caspases in the liver of MUP-core mice treated with isotype control ($n = 4$, blue histograms and dots) or αNK1.1 Abs ($n = 4$, red histograms and dots). A positive control for caspase activation in Cor93 T$_E$ cells upon in vitro UV exposure is indicated [left in (B)]. Endogenous CD8$^+$ T cells (Endo CD8) are indicated with dashed line as reference. Data are representative of at least three independent experiments. (**D**) Splenocytes isolated from Cor93 TCR transgenic mice (Cor93 TCR Tg) were pulsed in vitro with the cognate peptide Cor$^{93–100}$. Two and 3 days after peptide stimulation, Cor93 T cells were retrovirally transduced with a FRET-based fluorescent probe (DEVD) sensitive to caspase-3 activity. As control, Cor93 T cells were retrovirally transduced with a control probe (DEVG) not sensitive to caspase-3 activity. Cor93 T cells were cultured for three more days to allow for effector differentiation before analyses or injection into recipient mice [see (E)]. (**E**) NKp46$^{iCre+/–}$; R26$^{iDTR+/–}$; MUP-core mice were injected with DT or PBS the day before and the day after receiving 10^7 Cor93 T$_E$ cells transduced with the DEVD or DEVG probe. Livers were collected and analyzed 36 hours after Cor93 T$_E$ transfer. (**F**) Percentage of apoptotic CFP$^+$ cells on DEVD-transduced Cor93 T$_E$ recovered from the liver of PBS- (blue dots, $n = 4$) or DT-treated mice (red dots, $n = 5$). Control mice that received DEVG-transduced Cor93 T$_E$ are shown (black dots, $n = 3$). (**G**) The apoptotic index of DEVD-transduced Cor93 T$_E$ in mice treated with DT or PBS. Control mice that received DEVG-transduced Cor93 T$_E$ are shown (black dots, $n = 3$). Data are representative of at least two independent experiments. (**H**) MUP-core mice were lethally irradiated and received *Perforin* (*Prf*$^{–/–}$) or C57BL/6 (WT) BM. After 8 weeks, mice were treated with αNK1.1 Abs or isotype control before receiving 10^7 Cor93 T$_E$. Livers were collected and analyzed 3 days after T cell transfer. (**I** to **K**) Absolute numbers of group 1 ILCs (I), Cor93 T$_E$ cells (J), and IFN-γ$^+$ Cor93 T$_E$ (K) in the liver of indicated mice 3 days after T cell transfer (*Prf*$^{–/–}$, empty symbols, $n = 5$; WT, filled symbols, $n = 4$). Data are representative of at least two independent experiments. Normal distribution was verified by Shapiro-Wilk test. (**L**) MUP-core mice were lethally irradiated and received *Ncr1*$^{–/–}$ or WT BM. After 8 weeks, mice were treated with αNK1.1 Abs or isotype control before receiving 10^7 Cor93 T$_E$. Livers were collected and analyzed 3 days after T cell transfer. (**M** to **O**) Absolute numbers of group 1 ILCs (M), Cor93 T$_E$ (N), and IFN-γ$^+$ Cor93 T$_E$ (O) in the liver of indicated mice 3 days after T cell transfer (*Ncr1*$^{–/–}$, empty symbols, $n = 4$; WT, filled symbols, $n = 4$). Data are representative of at least two independent experiments. Normal distribution was verified by Shapiro-Wilk test. Data are expressed as means ± SEM. *$P < 0.05$, **$P < 0.01$, and ***$P < 0.001$; two-tailed Mann-Whitney *U* test (C), Kruskal-Wallis test (F and G), and one-way ANOVA with Sidak's multiple comparisons test (I to K and M to O).

equally in the two transplanted groups and were significantly reduced by αNK1.1 treatment (Fig. 4M). *Ncr1*$^{-/-}$ NK cells were equivalent to WT NK cells in their ability to limit the intrahepatic accumulation of IFN-γ–producing Cor93 T_E (Fig. 4, N and O) and the attendant immunopathology (fig. S5B). In summary, our results do not support the hypothesis that group 1 ILCs restrain T cell–mediated liver immunopathology by inducing T cell apoptosis.

Group 1 ILCs limit the proliferation of HBV-specific CD8$^+$ T_E cells

We then hypothesized that group 1 ILCs might modulate hepatic T cell immunity by interfering with T cell proliferation. To test this, we adoptively transferred CellTrace Violet (CTV)–labeled Cor93 T_E to group 1 ILC-depleted or control MUP-core mice (Fig. 5A). As shown previously, the number of intrahepatic Cor93 T_E was higher in αNK1.1-treated mice compared with isotype control–treated animals (Fig. 5B). This higher intrahepatic accumulation was associated with a higher CTV dilution, indicative of increased Cor93 T_E proliferation (Fig. 5C). When we tracked cell generations, we found a higher proliferation index (the total number of cell divisions divided by the number of cells that went into division) in Cor93 T_E isolated from αNK1.1-treated MUP-core mice compared with isotype control–treated animals (Fig. 5, D to F). These data support a role for group 1 ILCs in regulating the proliferation of intrahepatic CD8$^+$ T_E cells undergoing hepatocellular antigen recognition.

Group 1 ILCs restrain CD8$^+$ T_E cell proliferation by competing for local IL-2 availability

Because T cell proliferation requires IL-2 (*41*) and group 1 ILCs express the high-affinity receptor for this cytokine (Fig. 6A) (*3*, *42*), we next hypothesized that hepatic group 1 ILCs might regulate T cell proliferation by depriving CD8$^+$ T_E cells of access to IL-2. To explore this possibility, we genetically removed the IL-2 receptor α subunit (IL-2Rα also known as CD25) from group 1 ILCs. The resulting NKp46^{iCre};CD25$^{fl/fl}$ mice were further bred against MUP-core mice. We confirmed that, when compared with NKp46^{iCre};MUP-core mice, NKp46^{iCre};CD25$^{fl/fl}$;MUP-core mice lacked CD25 expression on group 1 ILCs (Fig. 6, B and C). The genetic absence of IL-2Rα from group 1 ILCs did not affect the total number of hepatic group 1 ILCs (Fig. 6D) but slightly decreased the number of ILC1s (Fig. 6E) without significantly modifying their surface expression of key molecules including CD127, IL-18R1, programmed cell death protein 1 (PD-1), and TNF-related apoptosis-inducing ligand (TRAIL) in vitro or their ability to secrete IFN-γ in vivo (fig. S6, A to G). Next, we injected NKp46^{iCre};CD25$^{fl/fl}$;MUP-core mice (and NKp46^{iCre};MUP-core controls) with αNK1.1-depleting Ab or isotype control before Cor93 T_E transfer (Fig. 6F). The genetic ablation of IL-2Rα from group 1 ILCs did not significantly affect the total group 1 ILC accumulation within the liver upon T_E injection; however, it slightly increased the NK/ILC1 ratio (Fig. 6, G to I). When we examined the number of Cor93 T_E (and their IFN-γ–producing capacity), we observed that the genetic deficiency of IL-2Rα in group 1 ILCs phenocopied the effect of group 1 ILC depletion (Fig. 6, J and K). Further, the injection of αNK1.1-depleting Ab in NKp46^{iCre};CD25$^{fl/fl}$;MUP-core mice failed to have an additional effect (Fig. 6, J and K). Together, the results indicate that the capacity of group 1 ILCs to hinder Cor93 T_E proliferation requires their expression of the high-affinity receptor for IL-2.

To distinguish between NK cells and ILC1s, we transplanted NKp46^{iCre};R26^{tdTomato};Eomes^{Gfp} BM into irradiated MUP-core recipients (Fig. 6L). In the resulting mice, ILC1s (Tomato$^+$) can be distinguished from NK cells (Tomato$^+$/Eomes^{Gfp+}). Whereas both NK cells and ILC1s were found to crawl along liver sinusoids (Fig. 6M), we found that ~80% of the interactions between Cor93 T_E and group 1 ILCs involved ILC1s rather than NK cells (Fig. 6, N and O, and movie S3). Together with a higher expression of CD25 (Fig. 6A), the data suggest that ILC1s (more than NK cells) limit T cell–induced liver immunopathology by competing for local IL-2 availability.

We recently proposed IL-2–based immunotherapeutic strategies to revert the CD8$^+$ T cell dysfunction induced by hepatocellular priming (*43*, *44*). We then reasoned that, by competing for local IL-2 availability, hepatic group 1 ILCs might hinder the therapeutic efficacy of IL-2. To test this hypothesis, HBV Tg mice were treated with αNK1.1-depleting Ab before the adoptive transfer of Cor93 naïve CD8$^+$ T cells (Cor93 T_N). One day after transfer, selected mice received IL-2 (Fig. 6P). As previously described (*43*, *44*), IL-2 administration to HBV Tg mice resulted in Cor93 T cell expansion and differentiation into IFN-γ–producing, cytotoxic effector cells and in NK cell and ILC1 expansion (Fig. 6, Q to S). Group 1 ILC depletion alone failed to improve the number and/or function of Cor93 T cells undergoing hepatocellular antigen recognition (Fig. 6, T to V). However, group 1 ILC depletion increased the capacity of IL-2 to promote Cor93 T cell expansion and differentiation into IFN-γ–producing, cytotoxic effector cells (Fig. 6, T to V). Together, these results support the hypothesis that hepatic group 1 ILCs compete with CD8$^+$ T_E cells for the local availability of IL-2 (either produced by T cells or exogenously administered).

DISCUSSION

In this study, we have used static and dynamic imaging, high-dimensional flow cytometry, and functional experiments to delineate the role of ILCs in mouse models of HBV pathogenesis. We report that group 1 ILCs actively crawl along liver sinusoids, and they engage in prolonged interactions with HBV-specific CD8$^+$ T_E cells undergoing hepatocellular antigen recognition. However, contrary to what was previously reported in other settings, we found no evidence of hepatic group 1 ILCs directly killing activated T cells; rather, they deprived CD8$^+$ T_E cells of access to IL-2, thus restraining their proliferation. Accordingly, depleting group 1 ILCs, or impairing their capacity to sense IL-2, increases the number of intrahepatic HBV-specific CD8$^+$ T_E cells and the attendant immunopathology.

In light of their enrichment in the liver and of their increase upon T cell–mediated immunopathology both in mice (*45*) and in humans (*46*), group 1 ILCs have been previously suggested to play a role in HBV pathogenesis (*7*). For instance, hepatic group 1 ILCs could contribute to HBV-induced liver damage by directly killing hepatocytes through a number of effector mechanisms, e.g., perforin/granzyme (*14*, *47*, *48*), Fas ligand (*49*–*52*), TNF superfamily (*53*, *54*), and TRAIL (*15*, *55*, *56*). However, in vivo killing of hepatocytes by group 1 ILCs during HBV-induced liver immunopathology has not been demonstrated and it is not supported by the data reported in this manuscript. Group 1 ILCs are known producers of IFN-γ (*5*) and thus could potentially be involved in the noncytopathic inhibition of HBV replication (*16*). Previous experiments in transgenic mice and in experimentally infected chimpanzees, however, suggested

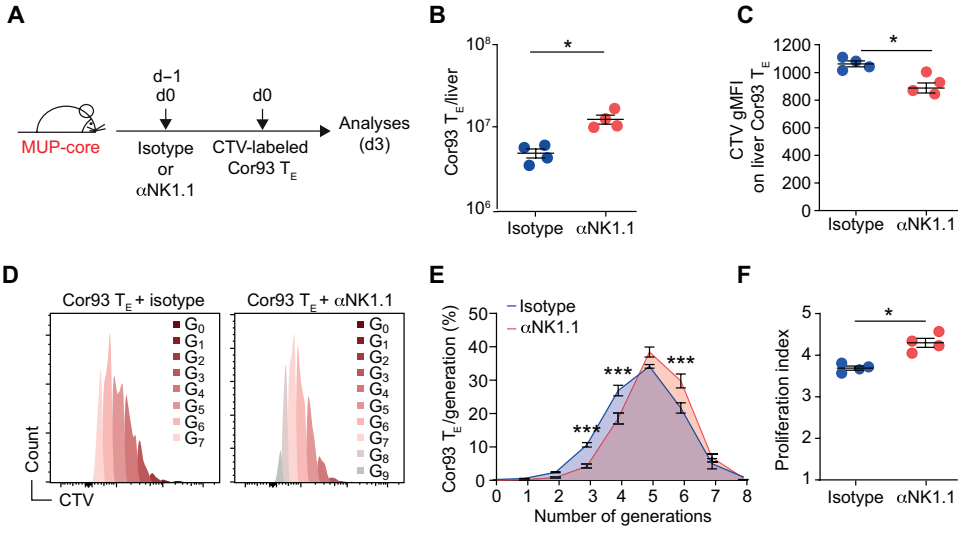

Fig. 5. Group 1 ILCs limit HBV-specific CD8$^+$ T_E cell proliferation. (**A**) Schematic representation of the experimental setup. MUP-core mice were injected with αNK1.1 Abs or isotype control before the transfer of 10^7 CTV-labeled Cor93 T_E. Livers were collected and analyzed 3 days after T cell transfer. (**B**) Absolute numbers of Cor93 T_E in the liver of mice treated with αNK1.1 (αNK1.1; $n = 4$, red dots) or isotype control ($n = 4$, blue dots). (**C**) Quantification of the geometric mean fluorescent intensity (gMFI) of CTV expression by Cor93 T_E in the liver of the indicated mice 3 days after T cell transfer. (**D**) Representative histograms of CTV-labeled Cor93 T_E obtained from the liver of isotype control–(left) or αNK1.1-treated (right) mice 3 days after T_E transfer. Each peak represents a cell division and is indicated with a different color. (**E**) Percentage of Cor93 T_E in each cell division [gated as shown in (D)] from isotype control– (blue line) or αNK1.1-treated (red line) mice 3 days after T_E transfer. (**F**) Proliferation index, defined as the total number of divisions divided by the number of cells that went into division, of Cor93 T_E cells obtained from the liver of the indicated mice 3 days after T cell transfer. Data are expressed as means ± SEM and are representative of at least two independent experiments. *$P < 0.05$ and ***$P < 0.001$; two-tailed Mann-Whitney U test (B, C, and F) and two-way ANOVA followed by Sidak's multiple comparisons test, stars indicate significant differences among groups per each generation (E).

that the contribution of group 1 ILC-derived IFN-γ to HBV clearance is probably marginal (compared with the much larger amount produced by HBV-specific CD8$^+$ T_E cells) (*45*, *57*, *58*). Moreover, in patients chronically infected by HBV, group 1 ILCs become defective in their production of IFN-γ (*14*, *47*, *59*), rendering them ineffective at exerting antiviral functions (*7*). Finally, data obtained over the last decade indicate that group 1 ILCs can either stimulate or inhibit CD8$^+$ T cell responses (*17*). Enhancement of CD8$^+$ T cell responses occurs mostly via indirect mechanisms, owing to the capacity of group 1 ILC-derived cytokines (e.g., IFN-γ) to promote dendritic cell maturation (*60*–*63*). This aspect of group 1 ILC biology was not addressed in this study, because the experimental systems used herein do not rely on in vivo CD8$^+$ T cell priming. More recently, group 1 ILCs have been shown to limit CD8$^+$ T cell responses directly by their ability to recognize and kill activated T cells (*17*–*25*). The data presented here expand the role of group 1 ILCs in negatively regulating T cell responses, showing that they can do so by competing for the local availability of IL-2. By contrast, we saw no evidence of group 1 ILCs directly killing CD8$^+$ T cells. Possible explanations for this apparent discrepancy with earlier studies include that we used a fully immunocompetent mouse model [some earlier studies indicate that group 1 ILC cytotoxicity toward CD8$^+$ T cells occur if the latter lack type I IFN receptor signaling (*24*, *25*)], that we focused exclusively on the effector phase of the CD8$^+$ T cell response, or that the phenomenon described here is liver-specific and not occurring elsewhere (e.g., in secondary lymphoid organs).

Limiting effector T cell responses by reducing local IL-2 availability is a mechanism previously ascribed to T regulatory cells (*64*, *65*). We speculate that, in the liver, this regulatory function might be performed by group 1 ILCs, given their high abundance and the high trimeric (i.e., high-affinity) IL-2 receptor expression, particularly on ILC1s. Adaptive T cells have been proposed to progressively displace ILCs as a function of age and pathogen-driven perturbations (*2*). Hence, CD8$^+$ T cells might be competing for niches established during development by group 1 ILCs and likely use an overlapping array of signals (this study identifies IL-2 as one of them) for tissue occupancy. Further evidence of a competition between group 1 ILCs and CD8$^+$ T cells is provided by the IL-2–dependent NK cell expansion observed upon lymphocytic choriomeningitis virus infection in mice lacking CD8$^+$ T cells (*66*).

This study has several limitations, including that it relies on the adoptive transfer of a relatively large number of TCR transgenic CD8$^+$ T cells. Second, although our data indicate that, when compared with NK cells, ILC1s interact more with CD8$^+$ T_E cells and express higher levels of CD25, we have not definitely resolved whether the T cell–limiting activity is restricted to ILC1s or whether NK cells contribute as well. In addition, we have focused our analyses on the impact of group 1 ILCs on CD8$^+$ T cells and have not addressed whether similar mechanisms are also operative in CD4$^+$ T cells. Last, we have not directly investigated the role of molecules such as TRAIL or PD-L1 that have been previously suggested to play a role in limiting T cell responses (*23*, *28*, *67*). We believe that future studies should confirm and extend our results, as well as address the abovementioned issues.

Several questions remain also unanswered that warrant further investigation. For instance, what causes the intrahepatic accumulation of group 1 ILCs upon T cell–mediated immunopathology? Previous studies suggest that CD8$^+$ T_E cell–derived IFN-γ induces the hepatic expression of chemokine (C-X-C motif) ligands 9 and 10 (CXCL9 and CXCL10), which recruit NK1.1$^+$ cells in a chemokine (C-X-C motif) receptor 3 (CXCR3)-dependent fashion (*45*). Furthermore, IFN-γ has been shown to promote the development of ILC1s from Lin$^-$ CD122$^+$ CD49a$^+$ progenitors (*68*). However, the relative role of recruitment versus local proliferation of either NK cells or ILC1s remains to be fully resolved. Further, what are the mechanisms whereby hepatic group 1 ILCs interact with CD8$^+$ T_E cells? Is the interaction mediated exclusively by the local sensing of IL-2, or are group 1 ILCs sensing additional chemoattractants produced by T cells? Are there adhesion molecules involved in the interaction? Answers to these questions will provide further insight into interactions between hepatic group 1 ILCs and CD8$^+$ T cells.

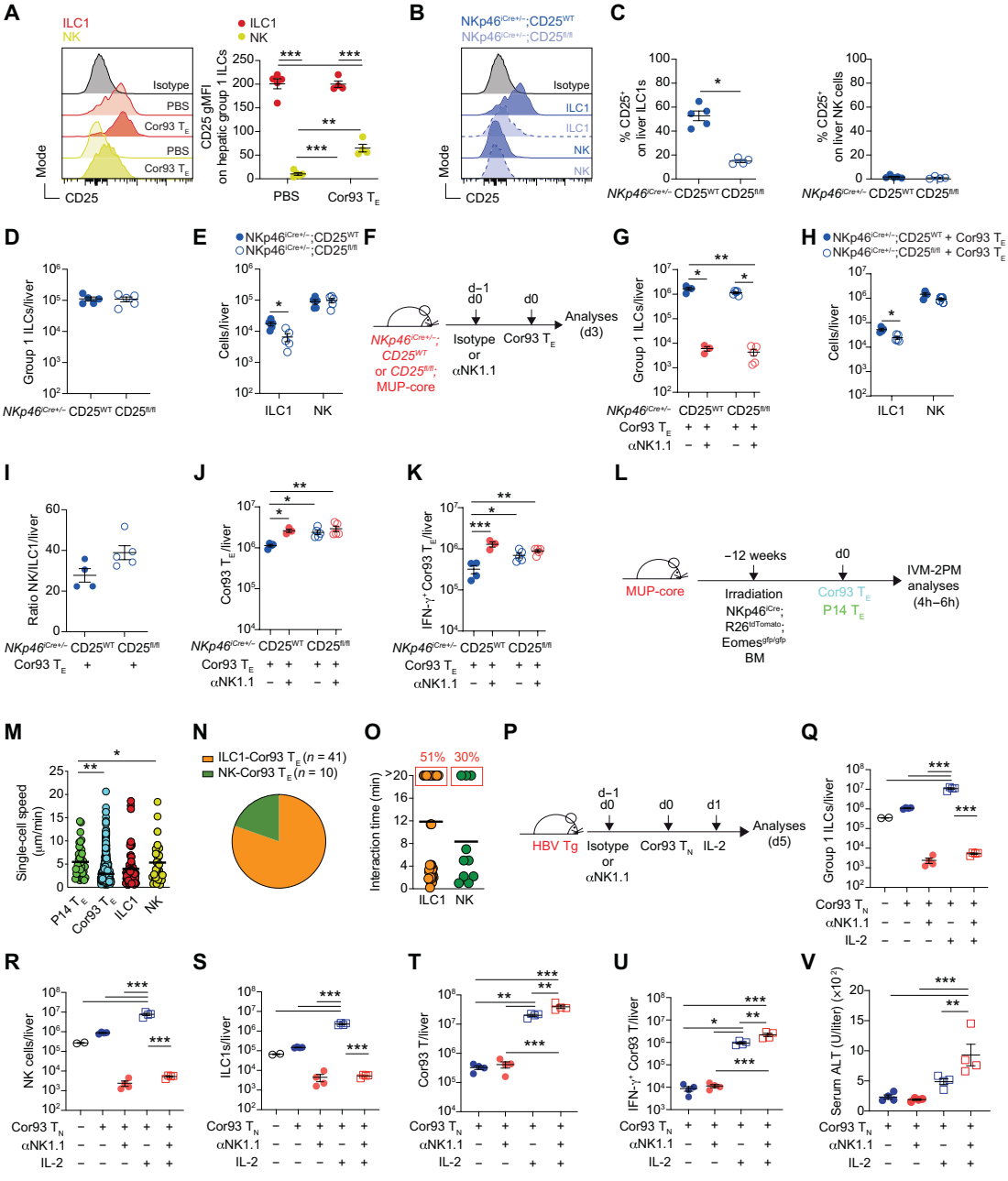

Fig. 6. Group 1 ILCs restrain CD8$^+$ T_E cell proliferation by competing for local IL-2 availability. (**A** and **B**) Representative histograms and geometric fluorescent intensity quantification of CD25 expression on ILC1s (red line and dots) and NK cells (yellow line and dots) in the liver of MUP-core mice upon PBS ($n = 5$) or Cor93 T_E injection ($n = 4$). As control, isotype control is indicated in gray. (**B**) Representative histograms of CD25 expression on ILC1s and NK cells in the liver of NKp46$^{iCre+/-}$; CD25^{WT}; MUP-core mice (blue line) or NKp46$^{iCre+/-}$; CD25$^{fl/fl}$; MUP-core mice (blue dashed line). (**C**) Frequency of CD25$^+$-ILC1s (left) and CD25$^+$-NK cells (right) in the liver of NKp46$^{iCre+/-}$; CD25^{WT}; MUP-core mice (filled symbols, $n = 5$) or NKp46$^{iCre+/-}$; CD25$^{fl/fl}$; MUP-core mice (empty symbols, $n = 4$). (**D** and **E**) Absolute numbers of group 1 ILCs (D), ILC1s, and NK cells (E) obtained from the liver of NKp46$^{iCre+/-}$; CD25^{WT}; MUP-core (filled symbols, $n = 5$) or NKp46$^{iCre+/-}$; CD25$^{fl/fl}$; MUP-core mice (empty symbols, $n = 5$). (**F**) NKp46$^{iCre+/-}$; CD25^{WT} or CD25$^{fl/fl}$; MUP-core mice were treated with αNK1.1 Abs or isotype control before receiving 10^7 Cor93 T_E. Livers were collected and analyzed 3 days after T cell transfer. (**G** and **H**) Absolute numbers of group 1 ILCs (G), ILC1s, and NK cells (H) obtained 3 days after T cell transfer from the liver of the indicated mice treated with αNK1.1 (red dots, $n = 3$ to 5) or isotype control (blue dots, $n = 4$ to 5). (**I**) Ratio between NK cells and ILC1s recovered from the liver of indicated mice 3 days after T cell transfer. (**J** and **K**) Absolute numbers of Cor93 T_E (J) and IFN-γ$^+$ Cor93 T_E (K) in the liver of the indicated mice 3 days after transfer. Data are expressed as means ± SEM and are representative of at least two independent experiments. (**L**) MUP-core mice were lethally irradiated and received NKp46$^{iCre+/-}$; R26$^{TdTomato+/-}$;Eomes$^{gfp/gfp}$ BM. After 12 weeks, mice were injected with 10^7 fluorescent Cor93 T_E (cyan) and 10^7 fluorescent control P14 T_E (green). Multiphoton intravital microscopy was performed from 4 to 6 hours after injection ($n = 4$). (**M**) The average cell velocity per track of indicated cells is represented. Circles represent a cell track, and bars indicate median values. A total of 109 NK tracks, 134 ILC1 tracks, 349 Cor93 T_E tracks, and 38 P14 T_E tracks were analyzed. (**N**) Pie chart representing the number of interactions between Cor93 T_E cells and ILC1s or NK cells. Eighty percent of interactions (n of interaction = 41, orange) are between Cor93 T_E and ILC1s; 20% of interactions are between Cor93 T_E and NK cells (n of interactions = 10; green). (**O**) Quantification of the interaction time between ILC1s (orange) or NK cells (green) and Cor93 T_E cells. Red boxes indicate the percentage of cells that are interacting for more than 20 min. Data are from four mice in two different experiments. (**P**) Schematic representation of the experimental setup. HBV Tg mice were injected with the αNK1.1 Abs ($n = 8$, red symbols) or isotype control ($n = 8$, blue symbols) before the transfer of 10^6 HBcAg-specific naïve CD8$^+$ T cells (Cor93 T_N) followed, 24 hours later, by administration of IL-2. Livers were collected and analyzed 5 days after T cell transfer. (**Q** to **S**) Absolute numbers of group 1 ILCs (Q), NK cells (R), and ILC1s (S) obtained 5 days after T cell transfer from the liver of the indicated mice that received IL-2 ($n = 8$, empty symbols) or PBS ($n = 8$, filled symbols). Control, untreated mice are shown as additional controls ($n = 2$, empty black symbols). (**T** and **U**) Absolute numbers of Cor93 T cells (T) and of IFN-γ$^+$ Cor93 T cells (U) in the liver of the indicated mice. (**V**) Serum transaminase activity (ALT; U/liter) in the indicated mice 3 days after Cor93 T_N injection. Data are expressed as means ± SEM and are representative of at least two independent experiments. *$P < 0.05$, **$P < 0.01$, and ***$P < 0.001$; two-tailed Mann-Whitney U test (C to E, H, and I), Kruskal-Wallis test (G, J, K, and M), and two-way ANOVA followed by Sidak's multiple comparisons test (A and Q to V).

In summary, we have revealed a role for hepatic group 1 ILCs in limiting liver immunopathology by restraining $CD8^+$ T_E cell proliferation through competition for local IL-2 availability. We believe that this work has potentially significant implications for immunotherapeutic approaches against chronic HBV infection, because hepatic group 1 ILCs might limit the therapeutic efficacy of conventional IL-2 therapy. In addition, strategies aimed at boosting the herein described function of group 1 ILCs might be considered to limit T cell–mediated organ damage.

MATERIALS AND METHODS

Study design

The aim of this study was to delineate the in vivo function of hepatic group 1 ILCs during T cell–mediated liver immunopathology. We sought to address this aim using two lineages of HBV Tg mice (HBV replication–competent and MUP-core mice) as recipients of HBV-specific $CD8^+$ T cells. Mouse experiments were planned in accordance with the principles of the 3Rs (replacement, reduction, and refinement). Liver immunopathology was assessed by measuring the level of serum transaminase and by characterizing the immune cell infiltrates in the liver through flow cytometry and histology. The intrahepatic behavior of group 1 ILCs and their cross-talk with $CD8^+$ T cells were analyzed by intravital microscopy and confocal immunofluorescence histology. The capacity of group 1 ILCs to compete for local IL-2 was demonstrated by genetically removing the IL-2Rα from group 1 ILCs. Sample size and replicates for each experiment are indicated in the figure legends. During analysis, no individual data points were excluded under any circumstances other than technical failure to process the sample. Animals were randomized to the experimental groups.

Mouse models

C57BL/6, CD45.1 (inbred C57BL/6), Balb/c, Thy1.1 [CBy.PL(B6)-*Thy*^{a}/ScrJ], β-actin–green fluorescent protein (GFP) [C57BL/6-Tg(CAG-EGFP)1Osb/J], Ai14(RCL-TdT) [B6.Cg-Gt(ROSA)26Sor$^{tm14(CAG-TdTomato)Hze}$/J], Ai6(RCL-ZsGreen) [B6.Cg-Gt(ROSA)26Sor$^{tm6(CAG-ZsGreen1)Hze}$/J], and B6(129S4)-Il2ra$^{tm1c(EUCOMM)Wtsi}$/TrmaJ mice were purchased from Charles River or the Jackson Laboratory. ROSA26 (R26)^{iDTR} mice (*69*) were obtained from M. Bacigaluppi (San Raffaele Scientific Institute). NKp46^{iCre} knock-in mice (inbred C57BL/6), in which *iCre* was inserted by homologous recombination at the 3′ end of the *NKp46* gene, have been previously described (*29*). In indicated experiments, NKp46^{iCre} mice were bred against R26^{TdTomato}, R26^{ZsGreen}, CD25$^{fl/fl}$, or R26^{iDTR} mice. MUP-core transgenic mice (lineage MUP-core 50 [MC50], inbred C57BL/6), which express the HBV core protein in 100% of the hepatocytes under the transcriptional control of the mouse MUP promoter, have been previously described (*34*). In selected experiments, MUP-core mice were bred against NKp46^{iCre};R26^{TdTomato} mice, against NKp46^{iCre};R26^{iDTR} or against NKp46^{iCre};CD25$^{fl/fl}$ mice. HBV Tg mice (lineage 1.3.32, inbred C57BL/6), which express all of the HBV antigens and replicate HBV in the liver at high levels without any evidence of cytopathology, have been previously described (*26*). In indicated experiments, HBV Tg mice were used as C57BL/6 × Balb/c (H-2^{bxd}) F_1 hybrids. Cor93 TCR transgenic mice (lineage BC10.3, inbred CD45.1), in which >98% of the splenic $CD8^+$ T cells recognize a K^b-restricted epitope located between residues 93 and 100 in the HBV core protein (MGLKFRQL), have been previously described (*33*). For imaging experiments, Cor93 transgenic mice were bred against β-actin–GFP. Env28 TCR transgenic mice (lineage 6C2.36, inbred Balb/c), in which ~83% of the splenic $CD8^+$ T cells recognize a L^d-restricted epitope located between residues 28 and 39 of HBsAg (IPQSLDSWWTSL), have been previously described (*33*). They were mated once with Thy1.1 mice (inbred Balb/c) so that the TCR transgenic T cells could be easily followed upon adoptive transfer by anti-Thy1.1 Ab staining. P14 mice (*70*) were obtained through the Swiss Immunological Mouse Repository. Mice were housed under specific pathogen–free conditions and used at 8 weeks of age, unless otherwise indicated. In all experiments, male mice were matched for age and (for HBV replication–competent mice) serum HBeAg levels before experimental manipulations. All experimental animal procedures were approved by the Institutional Animal Committee of the San Raffaele Scientific Institute.

Naïve $CD8^+$ T cell isolation, $CD8^+$ T_E cell differentiation, and adoptive transfer

Naïve $CD8^+$ T cells were differentiated in vitro for 7 to 9 days into effector cells before adoptive transfer (10^7 effector cells per mouse), as described (*30*). Briefly, splenocytes from Env28, Cor93, or P14 TCR transgenic mice were incubated at 37°C for 1 hour with Env$^{28–39}$ (L^d; IPQSLDSWWTSL), Cor$^{93–100}$ (K^b; MGLKFRQL), or GP$^{33–41}$ (D^b; KAVYNFATM) (10 μg/ml) peptides (Primm), respectively. After stimulation, cells were washed and cultured in complete medium supplemented with IL-2 for 7 to 9 days. In imaging experiments, 10^7 effector P14 T cells were labeled with 1 μM Deep Red (Life Technologies, #C34565) for 20 min at 37°C in RPMI before adoptive transfer together with 10^7 effector Cor93 GFP$^+$ $CD8^+$ T cells. In the experiments described in Fig. 6, mice were adoptively transferred with 10^6 HBV-specific naïve $CD8^+$ TCR transgenic T cells isolated from the spleens of Cor93 TCR transgenic mice, as previously described (*43*).

T cell transduction

pMSCV-CFP-DEVD-YFP and pMSCV-CFP-DEVG-YFP plasmids were previously described (*36*). To produce retroviral particles, human embryonic kidney (HEK)–293T cells were cotransfected with 2 μg of pCL-Eco packaging vector (#NBP2-29540) and 3 μg of DEVD or DEVG plasmid using a jetPRIME transfection reagent (Polyplus-transfection SA, Illkirch, France; #114-15). The medium was removed 4 hours later and replaced with fresh complete medium. Supernatants containing retroviral particles were harvested at 24 hours and filtered using a 0.45-μm filter.

$CD8^+$ T cells were isolated from the spleen of Cor93 TCR transgenic mice, as described above, and activated for 1 hour in the presence of Cor$^{93–100}$. Two rounds of spin infection (1000*g* for 90 min at 32°C) were performed after 48 and 72 hours using retroviral supernatant supplemented with polybrene (8 μg/ml) (Sigma-Aldrich, #TR-1003). T cells were cultured and expanded for additional 48 hours in fresh medium in the presence of 2.5% EL-4 supernatant.

Irradiation and BM transplantation

BM chimeras were generated by lethal irradiation of MUP-core mice (background C57BL/6N CD45.1/CD45.2) with one dose of 900 rad and reconstitution with the indicated BM (CD45.2); mice were allowed to reconstitute for at least 8 weeks before experimental manipulations. In the experiments described in Fig. 4, MUP-core mice were irradiated and reconstituted for at least 8 weeks with BM from *Perforin* (*Prf*$^{-/-}$) or *NKp46* (*Ncr1*$^{-/-}$) mice. In the experiments

described in Fig. 6, MUP-core mice were irradiated and reconstituted for at least 12 weeks with BM from *NKp46*$^{iCre+/-}$;R26$^{tdTomato+/-}$; Eomes$^{gfp/gfp}$ mice.

In vivo treatment

Group 1 ILCs were depleted by intravenous injection of αNK1.1-depleting Abs (100 μg per mouse; Bio X Cell, #BE0036, clone PK136) in HBV Tg mice or MUP-core mice. In selected experiments, NKp46$^{iCre+/-}$;R26^{iDTR} mice were treated intraperitoneally with 500 ng per mouse of DT (Millipore, #322326) 1 day before T cell transfer and every 48 hours. In selected experiments, HBV Tg mice were injected intraperitoneally with 0.5 mg/kg of an Fc effector dead WT IL-2 fusion protein, 1 day after HBV-specific naïve CD8$^+$ T cell transfer. In the experiments described in fig. S6, NKp46$^{iCre+/-}$; CD25^{WT} or NKp46$^{iCre+/-}$;CD25$^{fl/fl}$ mice were infected intraperitoneally with 10^3 plaque-forming units of murine cytomegalovirus (MCMV) (Smith strain), which was obtained from the lysate of salivary gland of BALB/c mice 3 weeks after infection.

Cell isolation and flow cytometry

Single-cell suspension of livers was generated as described (*43*). The lung was perfused through the right ventricle with PBS at the time of autopsy. Lung tissue was digested in RPMI 1640 containing collagenase IV (3.2 mg/ml) and deoxyribonuclease I (DNAse I) (25 U/ml) for 30 min at 37°C. The homogenized lung was passed through 70-μm nylon mesh to obtain a single-cell suspension. Cells were resuspended in 36% Percoll solution and centrifuged for 20 min at 2000 rpm (light acceleration and low brake). The remaining red blood cells were removed with ammonium-chloride-potassium (ACK) lysis. The small intestine was harvested paying attention to remove fat and Peyer's patches. It was cut longitudinally and rinsed with PBS and then it was placed in complete medium [Dulbecco's modified Eagles' medium supplemented with 10% fetal bovine serum (FBS), 1% penicillin and streptomycin, and 1% L-glutamine] with 1 mM dithiothreitol (Sigma-Aldrich, #10197777001) for 10 min at 37°C. The pieces of small intestine were then transferred in complete medium with 1 mM EDTA for 10 min at 37°C. After that, the EDTA buffer was replaced with a fresh one for other 10 min at 37°C. Tissue suspension was placed in fresh medium with collagenase D (1 mg/ml) (Sigma-Aldrich, #11088858001) and DNase I (5 U/ml) for 30 min at 37°C. The homogenized intestine was passed through 70-μm strainer and washed one time with PBS. Cell suspension was resuspended with 44% Percoll solution and overlaid on 66% Percoll solution. After centrifugation for 20 min at 2000 rpm (light acceleration and low brake), cells were isolated at the interface.

In selected experiments (fig. S6), IHLs were in vitro–stimulated for 4 hours with IL-12 (10 ng/ml) and IL-18 (10 ng/ml). For analysis of ex vivo intracellular cytokine production, brefeldin A (1 μg/ml) (Sigma-Aldrich) was included in the digestion buffer and in the stimulation cocktail. All flow cytometry stainings of surface-expressed and intracellular molecules were performed as described (*43*). Cell viability was assessed by staining with a Viobility 405/520 fixable dye (Miltenyi, no. 130-109-814). Abs used are indicated in table S1.

In selected experiments (Fig. 5), cells were labeled using a CTV cell proliferation kit (Thermo Fisher Scientific, #C34571) according to the manufacturer's instructions. The CaspGLOW Fluorescein Active Caspase Staining Kit (BioVision, #K180) was used for detecting activated caspases in living cells (Fig. 4). The assay uses the caspase family inhibitor VAD-FMK conjugated to FITC (FITC-VAD-FMK) that irreversibly binds to activated caspases. In selected experiments (Fig. 4 and fig. S4), the ratio of CFP to YFP fluorescence in transduced cells was calculated using FlowJo. Recombinant dimeric H-2Ld:Ig and H-2Kb:Ig fusion proteins (BD Biosciences) complexed with peptides derived from HBsAg (Env$^{28-39}$, IPQSLDSWWTSL, Primm) or from HBcAg (Cor$^{93-100}$, MGLKFRQL, Primm), respectively, were prepared according to the manufacturer's instructions. Flow cytometry analysis was performed on BD FACSCanto II or BD FACSymphony A5 and analyzed with FlowJo software (Treestar).

Confocal immunofluorescence histology

Livers were perfused with PBS, harvested and fixed in 4% paraformaldehyde for 16 hours, and then dehydrated in 30% sucrose before embedding in optimal cutting temperature compound (OCT) freezing media (Killik Bio-Optica, #05-9801). Twenty-micrometer sections were cut on a CM1520 cryostat (Leica) and adhered to Superfrost Plus slides (Thermo Fisher Scientific). Sections were then permeabilized and blocked in PBS containing 0.3% Triton X-100 (Sigma-Aldrich) and 10% FBS followed by staining in the same blocking buffer (*30*). The following primary Abs were used for staining: anti–collagen IV (polyclonal; Abcam, #Ab6586) and anti–Lyve-1 (polyclonal; Novus Biologicals, #NB600-1008). The following secondary Abs were used for staining: Alexa Fluor 647–conjugated goat anti-rabbit immunoglobulin G (IgG) (Life Technologies) and BV421-conjugated donkey anti-rabbit IgG (Life Technologies). Stained slides were mounted with the FluorSave Reagent (Merck Millipore, #345789), and images were acquired on an SP5 or SP8 confocal microscope (Leica Microsystem) with 40× oil-immersion or 20× objective. To minimize fluorophore spectral spillover, the Leica sequential laser excitation and detection modality was used.

Histochemistry

For hematoxylin and eosin (H&E) staining, livers were perfused with PBS, harvested in Zn formalin, and transferred into 70% ethanol 24 hours later. Tissues were then processed, embedded in paraffin, and stained as previously described (*30*, *43*). Bright-field images were acquired through an Aperio Scanscope System CS2 microscope and an ImageScope program (Leica Biosystem) following the manufacturer's instructions.

Multiphoton intravital microscopy

Liver multiphoton intravital microscopy was performed as described (*71*). Liver sinusoids were visualized by injecting nontargeted Qdot 655 (Life Technologies, #Q21021MP) intravenously immediately before imaging. Images were acquired with a LaVision BioTec TriMScope II coupled to a Nikon Ti-U inverted microscope enclosed in a custom-built environmental chamber (Life Imaging Services) that was maintained at 37° to 38°C with heated air. Fluorescence excitation was provided by two tunable femtosecond-pulsed Ti:Sa lasers (680 to 1080 nm; Ultra II, Coherent). The setup includes four photomultiplier tubes [three Hamamatsu H7422-40 GaAsP High Sensitivity photomultiplier tubes (PMTs) and one Hamamatsu H7422-50 GaAsP High Sensitivity red-extended PMT] and a high working distance water-immersion 25× objective (numerical aperture = 0.95; Olympus). For four-dimensional (4D) analysis of cell migration, stacks of 6 to 15 square *xy* sections (150 μm by 150 μm to 400 μm by 400 μm) sampled with 4-μm *z* spacing were acquired every 20 s for 20 to 60 min. Sequences of image stacks were

transformed into volume-rendered, 4D time-lapse movies with Imaris 8.4 and 9.1 (Bitplane). The 3D positions of the cell centroids were segmented by the semiautomated cell tracking algorithm of Imaris. The single-cell speed was calculated as the mean 3D velocity per cell track, whereas the instantaneous velocity represents the 3D velocities of each single step in a track. The arrest coefficient was defined as the percentage of time a track instantaneous velocity remains below a given motility threshold (here, 3 μm/min). The track displacement (distance between the initial and the final position of a cell) was divided by the total track length to obtain the meandering index, a measure of the directionality of a track. Last, mean displacement versus time and turning angle changes were calculated from the x, y, and z coordinates of the cell centroids using custom-designed scripts in MATLAB 2019b (MathWorks).

Biochemical analysis

The extent of hepatocellular injury was monitored by measuring plasma ALT activity at multiple time points after treatment, as previously described (*30*). Briefly, serum was obtained by centrifugation for 10 min at 3500 rpm. ALT/ glutamic pyruvic transaminase (GPT) liquid (#0018257440) was used for the quantitative determination of the serum ALT with an International Federation of Clinical Chemistry and Laboratory Medicine–optimized kinetic ultraviolet (UV) method in an ILab Aries chemical analyzer (Instrumentation Laboratory). SeraChem Control Level 1 and Level 2 (#0018162412 and #0018162512) were analyzed as quality control.

Statistical analyses and software

Detailed information concerning the statistical methods used is provided in the figure legends. Flow and imaging data were collected using FlowJo version 10.5.3 (Treestar) and Imaris (Bitplane), respectively. Statistical analyses were performed with GraphPad Prism software version 8 (GraphPad). n represents individual mice analyzed per experiment. Experiments were performed independently at least twice to control for experimental variation. Error bars indicate the SEM. Normality of data distribution was tested in all graphs with a Shapiro-Wilk normality test, and parametric tests were chosen only when normality could be confirmed for each dataset. We used Mann-Whitney U tests to compare two groups with nonnormally distributed continuous variables and Kruskal-Wallis nonparametric test to compare three or more unpaired groups. We used two-way analysis of variance (ANOVA) followed by Sidak's multiple comparisons tests to analyze experiments with multiple groups and two independent variables. Significance is indicated as follows: $^{*}P < 0.05$, $^{**}P < 0.01$, and $^{***}P < 0.001$. Comparisons are not statistically significant unless indicated.

SUPPLEMENTARY MATERIALS

www.science.org/doi/10.1126/sciimmunol.abi6112
Figs. S1 to S6
Movies S1 to S3
Table S1
Data file S1
MDAR Reproducibility Checklist

View/request a protocol for this paper from *Bio-protocol*.

REFERENCES AND NOTES

1. M. Ebbo, A. Crinier, F. Vély, E. Vivier, Innate lymphoid cells: Major players in inflammatory diseases. *Nat. Rev. Immunol.* **17**, 665–678 (2017).
2. M. E. Kotas, R. M. Locksley, Why innate lymphoid cells? *Immunity* **48**, 1081–1090 (2018).
3. E. Vivier, D. Artis, M. Colonna, A. Diefenbach, J. P. D. Santo, G. Eberl, S. Koyasu, R. M. Locksley, A. N. J. McKenzie, R. E. Mebius, F. Powrie, H. Spits, Innate lymphoid cells: 10 years on. *Cell* **174**, 1054–1066 (2018).
4. D. Artis, H. Spits, The biology of innate lymphoid cells. *Nature* **517**, 293–301 (2015).
5. M. Colonna, Innate lymphoid cells: Diversity, plasticity, and unique functions in immunity. *Immunity* **48**, 1104–1117 (2018).
6. G. F. Sonnenberg, M. R. Hepworth, Functional interactions between innate lymphoid cells and adaptive immunity. *Nat. Rev. Immunol.* **19**, 599–613 (2019).
7. M. K. Maini, D. Peppa, NK cells: A double-edged sword in chronic hepatitis B virus infection. *Front. Immunol.* **4**, 57 (2013).
8. X. Ficht, M. Iannacone, Immune surveillance of the liver by T cells. *Sci. Immunol.* **5**, eaba2351 (2020).
9. L. G. Guidotti, F. V. Chisari, Immunobiology and pathogenesis of viral hepatitis. *Annu. Rev. Pathol. Mech. Dis.* **1**, 23–61 (2006).
10. M. K. Maini, A. R. Burton, Restoring, releasing or replacing adaptive immunity in chronic hepatitis B. *Nat. Rev. Gastroenterol. Hepatol.* **16**, 662–675 (2019).
11. G. C. Fanning, F. Zoulim, J. Hou, A. Bertoletti, Therapeutic strategies for hepatitis B virus infection: Towards a cure. *Nat. Rev. Drug Discov.* **18**, 827–844 (2019).
12. P. A. Revill, F. V. Chisari, J. M. Block, M. Dandri, A. J. Gehring, H. Guo, J. Hu, A. Kramvis, P. Lampertico, H. L. A. Janssen, M. Levrero, W. Li, T. J. Liang, S.-G. Lim, F. Lu, M. C. Penicaud, J. E. Tavis, R. Thimme; Members of the ICE-HBV Working Groups, P. Arbuthnot, P. A. Boonstra, K.-M. Chang, P.-J. Chen, D. Glebe, L. G. Guidotti, J. Fellay, C. Ferrari, L. Jansen, D. T. Y. Lau, A. S. Lok, M. K. Maini, W. Mason, G. Matthews, D. Paraskevis, J. Petersen, B. Rehermann, E.-C. Shin, A. Thompson, F. van Bömmel, F.-S. Wang, K. Watashi, H.-C. Yang, Z. Yuan, M.-F. Yuen, I.-H. S. G. Chairs, T. Block, V. Miller, U. Protzer, I.-H. S. Advisors, C. Bréchot, S. Locarnini, M. G. Peters, R. F. Schinazi, F. Zoulim, A global scientific strategy to cure hepatitis B. *Lancet Gastroenterol. Hepatol.* **4**, 545–558 (2019).
13. M. Iannacone, L. G. Guidotti, Immunobiology and pathogenesis of hepatitis B virus infection. *Nat. Rev. Immunol.* **22**, 19–32 (2021).
14. B. Oliviero, S. Varchetta, E. Paudice, G. Michelone, M. Zaramella, D. Mavilio, F. D. Filippi, S. Bruno, M. U. Mondelli, Natural killer cell functional dichotomy in chronic hepatitis B and chronic hepatitis C virus infections. *Gastroenterology* **137**, 1151–1160.e7 (2009).
15. C. Dunn, M. Brunetto, G. Reynolds, T. Christophides, P. T. Kennedy, P. Lampertico, A. Das, A. R. Lopes, P. Borrow, K. Williams, E. Humphreys, S. Afford, D. H. Adams, A. Bertoletti, M. K. Maini, Cytokines induced during chronic hepatitis B virus infection promote a pathway for NK cell–mediated liver damage. *J. Exp. Med.* **204**, 667–680 (2007).
16. L. G. Guidotti, F. V. Chisari, Noncytolytic control of viral infections by the innate and adaptive immune response. *Annu. Rev. Immunol.* **19**, 65–91 (2001).
17. J. Crouse, H. C. Xu, P. A. Lang, A. Oxenius, NK cells regulating T cell responses: Mechanisms and outcome. *Trends Immunol.* **36**, 49–58 (2015).
18. B. A. Rabinovich, J. Li, J. Shannon, R. Hurren, J. Chalupny, D. Cosman, R. G. Miller, Activated, but not resting, T cells can be recognized and killed by syngeneic NK cells. *J. Immunol.* **170**, 3572–3576 (2003).
19. C. Cerboni, A. Zingoni, M. Cippitelli, M. Piccoli, L. Frati, A. Santoni, Antigen-activated human T lymphocytes express cell-surface NKG2D ligands via an ATM/ATR-dependent mechanism and become susceptible to autologous NK- cell lysis. *Blood* **110**, 606–615 (2007).
20. K. Soderquest, T. Walzer, B. Zafirova, L. S. Klavinskis, B. Polić, E. Vivier, G. M. Lord, A. Martín-Fontecha, Cutting edge: CD8+ T cell priming in the absence of NK cells leads to enhanced memory responses. *J. Immunol.* **186**, 3304–3308 (2011).
21. S. N. Waggoner, R. T. Taniguchi, P. A. Mathew, V. Kumar, R. M. Welsh, Absence of mouse 2B4 promotes NK cell–mediated killing of activated CD8+ T cells, leading to prolonged viral persistence and altered pathogenesis. *J. Clin. Invest.* **120**, 1925–1938 (2010).
22. P. A. Lang, K. S. Lang, H. C. Xu, M. Grusdat, I. A. Parish, M. Recher, A. R. Elford, S. Dhanji, N. Shaabani, C. W. Tran, D. Dissanayake, R. Rahbar, M. Ghazarian, A. Brüstle, J. Fine, P. Chen, C. T. Weaver, C. Klose, A. Diefenbach, D. Häussinger, J. R. Carlyle, S. M. Kaech, T. W. Mak, P. S. Ohashi, Natural killer cell activation enhances immune pathology and promotes chronic infection by limiting CD8+ T-cell immunity. *Proc. Natl. Acad. Sci. U.S.A.* **109**, 1210–1215 (2012).
23. D. Peppa, U. S. Gill, G. Reynolds, N. J. W. Easom, L. J. Pallett, A. Schurich, L. Micco, G. Nebbia, H. D. Singh, D. H. Adams, P. T. F. Kennedy, M. K. Maini, Up-regulation of a death receptor renders antiviral T cells susceptible to NK cell–mediated deletion. *J. Exp. Med.* **210**, 99–114 (2013).
24. J. Crouse, G. Bedenikovic, M. Wiesel, M. Ibberson, I. Xenarios, D. Von Laer, U. Kalinke, E. Vivier, S. Jonjic, A. Oxenius, Type I interferons protect T cells against NK cell attack mediated by the activating receptor NCR1. *Immunity* **40**, 961–973 (2014).
25. H. C. Xu, M. Grusdat, A. A. Pandyra, R. Polz, J. Huang, P. Sharma, R. Deenen, K. Köhrer, R. Rahbar, A. Diefenbach, K. Gibbert, M. Löhning, L. Höcker, Z. Waibler, D. Häussinger, T. W. Mak, P. S. Ohashi, K. S. Lang, P. A. Lang, Type I interferon protects antiviral CD8+ T cells from NK cell cytotoxicity. *Immunity* **40**, 949–960 (2014).
26. L. G. Guidotti, B. Matzke, H. Schaller, F. V. Chisari, High-level hepatitis B virus replication in transgenic mice. *J. Virol.* **69**, 6158–6169 (1995).

27. T. Nabekura, L. Riggan, A. D. Hildreth, T. E. O'Sullivan, A. Shibuya, Type 1 innate lymphoid cells protect mice from acute liver injury via interferon-γ secretion for upregulating Bcl-xL expression in hepatocytes. *Immunity* **52**, 96–108.e9 (2019).
28. J. Zhou, H. Peng, K. Li, K. Qu, B. Wang, Y. Wu, L. Ye, Z. Dong, H. Wei, R. Sun, Z. Tian, Liver-resident NK cells control antiviral activity of hepatic T cells via the PD-1-PD-L1 axis. *Immunity* **50**, 403–417.e4 (2019).
29. E. Narni-Mancinelli, J. Chaix, A. Fenis, Y. M. Kerdiles, N. Yessaad, A. Reynders, C. Gregoire, H. Luche, S. Ugolini, E. Tomasello, T. Walzer, E. Vivier, Fate mapping analysis of lymphoid cells expressing the NKp46 cell surface receptor. *Proc. Natl. Acad. Sci. U.S.A.* **108**, 18324–18329 (2011).
30. L. G. Guidotti, D. Inverso, L. Sironi, P. Di Lucia, J. Fioravanti, L. Ganzer, A. Fiocchi, M. Vacca, R. Aiolfi, S. Sammicheli, M. Mainetti, T. Cataudella, A. Raimondi, G. Gonzalez-Aseguinolaza, U. Protzer, Z. M. Ruggeri, F. V. Chisari, M. Isogawa, G. Sitia, M. Iannacone, Immunosurveillance of the liver by intravascular effector CD8+ T cells. *Cell* **161**, 486–500 (2015).
31. F. Geissmann, T. O. Cameron, S. Sidobre, N. Manlongat, M. Kronenberg, M. J. Briskin, M. L. Dustin, D. R. Littman, Intravascular immune surveillance by CXCR6+ NKT cells patrolling liver sinusoids. *PLoS Biol.* **3**, e113 (2005).
32. H. A. McNamara, Y. Cai, M. V. Wagle, Y. Sontani, C. M. Roots, L. A. Miosge, J. H. O'Connor, H. J. Sutton, V. V. Ganusov, W. R. Heath, P. Bertolino, C. G. Goodnow, I. A. Parish, A. Enders, I. A. Cockburn, Up-regulation of LFA-1 allows liver-resident memory T cells to patrol and remain in the hepatic sinusoids. *Sci. Immunol.* **2**, eaaj1996 (2017).
33. M. Isogawa, J. Chung, Y. Murata, K. Kakimi, F. V. Chisari, CD40 activation rescues antiviral CD8+ T cells from PD-1-mediated exhaustion. *PLOS Pathog.* **9**, e1003490 (2013).
34. L. G. Guidotti, V. Martinez, Y. T. Loh, C. E. Rogler, F. V. Chisari, Hepatitis B virus nucleocapsid particles do not cross the hepatocyte nuclear membrane in transgenic mice. *J. Virol.* **68**, 5469–5475 (1994).
35. S.-H. Lee, K.-S. Kim, N. Fodil-Cornu, S. M. Vidal, C. A. Biron, Activating receptors promote NK cell expansion for maintenance, IL-10 production, and CD8 T cell regulation during viral infection. *J. Exp. Med.* **206**, 2235–2251 (2009).
36. B. Breart, F. Lemaître, S. Celli, P. Bousso, Two-photon imaging of intratumoral CD8+ T cell cytotoxic activity during adoptive T cell therapy in mice. *J. Clin. Invest.* **118**, 1390–1397 (2008).
37. K. R. Garrod, H. D. Moreau, Z. Garcia, F. Lemaître, I. Bouvier, M. L. Albert, P. Bousso, Dissecting T cell contraction in vivo using a genetically encoded reporter of apoptosis. *Cell Rep.* **2**, 1438–1447 (2012).
38. K. Pallmer, I. Barnstorf, N. S. Baumann, M. Borsa, S. Jonjic, A. Oxenius, NK cells negatively regulate CD8 T cells via natural cytotoxicity receptor (NCR) 1 during LCMV infection. *PLOS Pathog.* **15**, e1007725 (2019).
39. D. L. Ivanova, R. Krempels, S. L. Denton, K. D. Fettel, G. M. Saltz, D. Rach, R. Fatima, T. Mundhenke, J. Materi, I. R. Dunay, J. P. Gigley, NK cells negatively regulate CD8 T cells to promote immune exhaustion and chronic toxoplasma gondii infection. *Front. Cell. Infect. Microbiol.* **10**, 313 (2020).
40. P. A. Lang, S. Q. Crome, H. C. Xu, K. S. Lang, L. Chapatte, E. K. Deenick, M. Grusdat, A. A. Pandyra, V. I. Pozdeev, R. Wang, T. A. W. Holderried, H. Cantor, A. Diefenbach, A. R. Elford, D. R. McIlwain, M. Recher, D. Häussinger, T. W. Mak, P. S. Ohashi, NK cells regulate CD8+ T cell mediated autoimmunity. *Front. Cell. Infect. Microbiol.* **10**, 36 (2020).
41. W. Liao, J.-X. Lin, W. J. Leonard, Interleukin-2 at the crossroads of effector responses, tolerance, and immunotherapy. *Immunity* **38**, 13–25 (2013).
42. G. Gasteiger, A. Y. Rudensky, Interactions between innate and adaptive lymphocytes. *Nat. Rev. Immunol.* **14**, 631–639 (2014).
43. A. P. Bénéchet, G. D. Simone, P. D. Lucia, F. Cilenti, G. Barbiera, N. L. Bert, V. Fumagalli, E. Lusito, F. Moalli, V. Bianchessi, F. Andreata, P. Zordan, E. Bono, L. Giustini, W. V. Bonilla, C. Bleriot, K. Kunasegaran, G. Gonzalez-Aseguinolaza, D. D. Pinschewer, P. T. F. Kennedy, L. Naldini, M. Kuka, F. Ginhoux, A. Cantore, A. Bertoletti, R. Ostuni, L. G. Guidotti, M. Iannacone, Dynamics and genomic landscape of CD8+ T cells undergoing hepatic priming. *Nature* **574**, 200–205 (2019).
44. G. D. Simone, F. Andreata, C. Bleriot, V. Fumagalli, C. Laura, J. M. Garcia-Manteiga, P. D. Lucia, S. Gilotto, X. Ficht, F. F. D. Ponti, E. B. Bono, L. Giustini, G. Ambrosi, M. Mainetti, P. Zordan, A. P. Bénéchet, M. Ravà, S. Chakarov, F. Moalli, M. Bajenoff, L. G. Guidotti, F. Ginhoux, M. Iannacone, Identification of a Kupffer cell subset capable of reverting the T cell dysfunction induced by hepatocellular priming. *Immunity* **15**, 2089–2100.e8 (2021).
45. K. Kakimi, T. E. Lane, S. Wieland, V. C. Asensio, I. L. Campbell, F. V. Chisari, L. G. Guidotti, Blocking chemokine responsive to γ–2/interferon (IFN)-γ inducible protein and monokine induced by IFN-γ activity in vivo reduces the pathogenetic but not the antiviral potential of hepatitis B virus–specific cytotoxic T lymphocytes. *J. Exp. Med.* **194**, 1755–1766 (2001).
46. M. Maini, C. Boni, C. Lee, J. Larrubia, S. Reignat, G. Ogg, A. King, J. Herberg, R. Gilson, A. Alisa, R. Williams, D. Vergani, N. Naoumov, C. Ferrari, A. Bertoletti, The role of virus-specific CD8(+) cells in liver damage and viral control during persistent hepatitis B virus infection. *J. Exp. Med.* **191**, 1269–1280 (2000).
47. D. Peppa, L. Micco, A. Javaid, P. T. F. Kennedy, A. Schurich, C. Dunn, C. Pallant, G. Ellis, P. Khanna, G. Dusheiko, R. J. Gilson, M. K. Maini, Blockade of immunosuppressive cytokines restores NK cell antiviral function in chronic hepatitis B virus infection. *PLOS Pathog.* **6**, e1001227 (2010).
48. Z. Zhang, S. Zhang, Z. Zou, J. Shi, J. Zhao, R. Fan, E. Qin, B. Li, Z. Li, X. Xu, J. Fu, J. Zhang, B. Gao, Z. Tian, F. Wang, Hypercytolytic activity of hepatic natural killer cells correlates with liver injury in chronic hepatitis B patients. *Hepatology* **53**, 73–85 (2011).
49. J. Ogasawara, R. Watanabe-Fukunaga, M. Adachi, A. Matsuzawa, T. Kasugai, Y. Kitamura, N. Itoh, T. Suda, S. Nagata, Lethal effect of the anti-Fas antibody in mice. *Nature* **364**, 806–809 (1993).
50. P. Galle, W. Hofmann, H. Walczak, H. Schaller, G. Otto, W. Stremmel, P. Krammer, L. Runkel, Involvement of the CD95 (APO-1/Fas) receptor and ligand in liver damage. *J. Exp. Med.* **182**, 1223–1230 (1995).
51. A. Okazaki, N. Hiraga, M. Imamura, C. N. Hayes, M. Tsuge, S. Takahashi, H. Aikata, H. Abe, D. Miki, H. Ochi, C. Tateno, K. Yoshizato, H. Ohdan, K. Chayama, Severe necroinflammatory reaction caused by natural killer cell-mediated Fas/Fas ligand interaction and dendritic cells in human hepatocyte chimeric mouse. *Hepatology* **56**, 555–566 (2012).
52. Y. Zou, T. Chen, M. Han, H. Wang, W. Yan, G. Song, Z. Wu, X. Wang, C. Zhu, X. Luo, Q. Ning, Increased killing of liver NK cells by Fas/Fas ligand and NKG2D/NKG2D ligand contributes to hepatocyte necrosis in virus-induced liver failure. *J. Immunol.* **184**, 466–475 (2010).
53. H. Mizuhara, E. O'Neill, N. Seki, T. Ogawa, C. Kusunoki, K. Otsuka, S. Satoh, M. Niwa, H. Senoh, H. Fujiwara, T cell activation-associated hepatic injury: Mediation by tumor necrosis factors and protection by interleukin 6. *J. Exp. Med.* **179**, 1529–1537 (1994).
54. J. W. Fang, W. W. Shen, A. Meager, J. Y. Lau, Activation of the tumor necrosis factor-alpha system in the liver in chronic hepatitis B virus infection. *Am. J. Gastroenterol.* **91**, 748–753 (1996).
55. S.-J. Zheng, P. Wang, G. Tsabary, Y. H. Chen, Critical roles of TRAIL in hepatic cell death and hepatic inflammation. *J. Clin. Invest.* **113**, 58–64 (2004).
56. K. Takeda, Y. Hayakawa, M. J. Smyth, N. Kayagaki, N. Yamaguchi, S. Kakuta, Y. Iwakura, H. Yagita, K. Okumura, Involvement of tumor necrosis factor-related apoptosis-inducing ligand in surveillance of tumor metastasis by liver natural killer cells. *Nat. Med.* **7**, 94–100 (2001).
57. H. McClary, R. Koch, F. V. Chisari, L. G. Guidotti, Relative sensitivity of hepatitis B virus and other hepatotropic viruses to the antiviral effects of cytokines. *J. Virol.* **74**, 2255–2264 (2000).
58. R. Thimme, S. Wieland, C. Steiger, J. Ghrayeb, K. A. Reimann, R. H. Purcell, F. V. Chisari, CD8(+) T cells mediate viral clearance and disease pathogenesis during acute hepatitis B virus infection. *J. Virol.* **77**, 68–76 (2003).
59. E. T. T. L. Tjwa, G. W. van Oord, J. P. Hegmans, H. L. A. Janssen, A. M. Woltman, Viral load reduction improves activation and function of natural killer cells in patients with chronic hepatitis B. *J. Hepatol.* **54**, 209–218 (2011).
60. F. Gerosa, B. Baldani-Guerra, C. Nisii, V. Marchesini, G. Carra, G. Trinchieri, Reciprocal activating interaction between natural killer cells and dendritic cells. *J. Exp. Med.* **195**, 327–333 (2002).
61. R. Mocikat, H. Braumüller, A. Gumy, O. Egeter, H. Ziegler, U. Reusch, A. Bubeck, J. Louis, R. Mailhammer, G. Riethmüller, U. Koszinowski, M. Röcken, Natural killer cells activated by MHC class ILOW targets prime dendritic cells to induce protective CD8 T cell responses. *Immunity* **19**, 561–569 (2003).
62. C. Adam, S. King, T. Allgeier, H. Braumüller, C. Lüking, J. Mysliwietz, A. Kriegeskorte, D. H. Busch, M. Röcken, R. Mocikat, DC-NK cell cross talk as a novel CD4+ T-cell–independent pathway for antitumor CTL induction. *Blood* **106**, 338–344 (2005).
63. P. Krebs, M. J. Barnes, K. Lampe, K. Whitley, K. S. Bahjat, B. Beutler, E. Janssen, K. Hoebe, NK cell–mediated killing of target cells triggers robust antigen-specific T cell–mediated and humoral responses. *Blood* **113**, 6593–6602 (2009).
64. G. Gasteiger, W. Kastenmuller, Foxp3+ regulatory T-cells and IL-2: The moirai of T-cell fates? *Front. Immunol.* **3**, 179 (2012).
65. S. Z. Josefowicz, A. Rudensky, Control of regulatory T CELL lineage commitment and maintenance. *Immunity* **30**, 616–625 (2009).
66. H. C. Su, J. S. Orange, L. D. Fast, A. T. Chan, S. J. Simpson, C. Terhorst, C. A. Biron, IL-2-dependent NK cell responses discovered in virus-infected beta 2-microglobulin-deficient mice. *J. Immunol.* **153**, 5674–5681 (1994).
67. L. C. Alves, M. D. Berger, T. Koutsandreas, N. Kirschke, C. Lauer, R. Spörri, A. Chatziioannou, N. Corazza, P. Krebs, Non-apoptotic TRAIL function modulates NK cell activity during viral infection. *EMBO Rep.* **21**, e48789 (2020).
68. L. Bai, M. Vienne, L. Tang, Y. Kerdiles, M. Etiennot, B. Escalière, J. Galluso, H. Wei, R. Sun, E. Vivier, H. Peng, Z. Tian, Liver type 1 innate lymphoid cells develop locally via an interferon-γ–dependent loop. *Science* **371**, eaba4177 (2021).
69. T. Buch, F. L. Heppner, C. Tertilt, T. J. A. J. Heinen, M. Kremer, F. T. Wunderlich, S. Jung, A. Waisman, A Cre-inducible diphtheria toxin receptor mediates cell lineage ablation after toxin administration. *Nat. Methods* **2**, 419–426 (2005).
70. H. Pircher, K. Bürki, R. Lang, H. Hengartner, R. M. Zinkernagel, Tolerance induction in double specific T-cell receptor transgenic mice varies with antigen. *Nature* **342**, 559–561 (1989).

71. A. P. Benechet, L. Ganzer, M. Iannacone, Intravital microscopy analysis of hepatic T cell dynamics. *Methods Mol. Biol.* **1514**, 49–61 (2017).

Acknowledgments: We thank M. Mainetti, M. Freschi, C. Perucchini, E. Bono, M. Raso, and A. Fiocchi for technical support; M. Silva for secretarial assistance; and the members of the Iannacone laboratory for helpful discussions. Flow cytometry was carried out at FRACTAL, a flow cytometry resource and advanced cytometry technical applications laboratory established by the San Raffaele Scientific Institute. Confocal immunofluorescence histology was carried out at Alembic, an advanced microscopy laboratory established by the San Raffaele Scientific Institute and the Vita-Salute San Raffaele University. We would like to acknowledge the Ph.D. program in Basic and Applied Immunology and Oncology at Vita-Salute San Raffaele University, as V.F. and V.V. conducted this study as partial fulfillment of their Ph.D. in Molecular Medicine within that program.